Suppression of Tumor or Host Intrinsic CMTM6 Drives Antitumor Cytotoxicity in a PD-L1–Independent Manner

Yiru Long[1,2], Runqiu Chen[1,3], Xiaolu Yu[1,2], Yongliang Tong[1,2], Xionghua Peng[1], Fanglin Li[1,2], Chao Hu[1,3], Jianhua Sun[1,2], and Likun Gong[1,2,4]

ABSTRACT

CKLF-like MARVEL transmembrane domain-containing protein 6 (CMTM6) is known to be a regulator of membranal programmed death ligand 1 (PD-L1) stability and a factor associated with malignancy progression, but the effects and mechanisms of CMTM6 on tumor growth, as well as its potential as a target for therapy, are still largely unknown. Here, we show that CMTM6 expression increased with tumor progression in both patients and mice. Ablation of CMTM6 significantly reduced human and murine tumor growth in a manner dependent on T-cell immunity. Tumor CMTM6 suppression broke resistance to immune-checkpoint inhibitors and remodeled the tumor immune microenvironment, as specific antitumor cytotoxicity was enhanced and contributed primarily to tumor inhibition. Without the PD-1/PD-L1 axis, CMTM6 suppression still significantly dampened tumor growth dependent on cytotoxic cells. Furthermore, we identified that CMTM6 was widely expressed on immune cells. T-cell CMTM6 levels increased with sustained immune activation and intratumoral immune exhaustion and affected T cell–intrinsic PD-L1 levels. Host CMTM6 knockout significantly restrained tumor growth in a manner dependent on $CD8^+$ T cells and not entirely dependent on PD-L1. Thus, we developed and evaluated the antitumor efficacy of CMTM6-targeting adeno-associated virus (AAV), which effectively mobilized antitumor immunity and could be combined with various antitumor drugs. Our findings reveal that both tumor and host CMTM6 are involved in antitumor immunity with or without the PD-1/PD-L1 axis and that gene therapy targeting CMTM6 is a promising strategy for cancer immunotherapy.

Introduction

The development of antibodies specific for programmed death ligand 1 (PD-L1) represented an inspiring clinical milestone for the treatment of malignancies (1–5). Despite this, the mechanisms regulating PD-L1 continue to be investigated in depth with the aim of solving the resistance and other problems (6, 7). In 2017, a novel PD-L1–interacting protein, CKLF-like MARVEL transmembrane domain-containing protein 6 (CMTM6), was identified as a critical regulator of PD-L1 membranal stability in cancer cells (8, 9). Colocalizing with membranal PD-L1, CMTM6 prolongs the half-life of PD-L1 on the cell membrane by obstructing PD-L1 degradation via the endosome–lysosome degradation pathway (8) and the ubiquitin–proteasome degradation pathway (9).

CMTM6, which is located on chromosome 3, and the genes encoding seven other chemokine-like factor superfamily members were identified as new genes by homology search in 2003 (10). CMTM6 is an M-shaped four-transmembrane protein containing the MARVEL transmembrane domain (10–12). After the initial discovery of the ability of CMTMT6 to regulate PD-L1, this function was confirmed in monocytes (13) as well as in other types of cancer cells (14). Extensive clinical analysis also found a significant positive correlation between CMTM6 and PD-L1 expression in tumors (15–20). Increased CMTM6 levels in tumors are associated with shorter overall survival (OS) and recurrence in patients with a wide variety of cancer types, including glioma, head and neck squamous cell carcinoma, melanoma, hepatocellular carcinoma (HCC) and triple-negative breast cancer (TNBC; refs. 18, 19, 21–24). Although CMTM6/PD-L1 coexpression is associated with a poorer prognosis (20, 25–27), it is associated with a better prognosis when immune-checkpoint blockade (ICB) therapy is used (28–30). However, some contradictory findings have also been reported, indicating a complex role for CMTM6 in certain types of cancer such as non–small cell lung cancer (NSCLC; refs. 31–33).

Research on the biological functions of CMTM6 is still in its infancy. It is reported to promote cisplatin resistance through acting with enolase-1 to activate Wnt signaling (34). Exosomal CMTM6 derived from oral squamous cell carcinoma cells augments macrophage M2 differentiation by activating the ERK1/2 pathway (35). Studies also show that CMTM6 inhibits p21 ubiquitination (36), genomic stability (37), and the mTOR pathway (38) to influence tumor cell growth, and acts on vimentin to affect tumor cell migration and invasion (39). Hu-Antigen R (40) and neuropilin-1 (41) can affect the expression of CMTM6 at the transcription and protein levels, respectively. In addition to oncology-related studies, researchers have found that Schwann cells optimize neural function by limiting axon diameter through CMTM6 (42).

In-depth and systematic research is urgently required to further elucidate the functions of CMTM6 in tumor progression. In this study, we extensively investigated the role and mechanism of human/mouse tumor CMTM6 as well as host cell CMTM6 in tumor immunity and explored the antitumor efficacy of gene therapy targeting CMTM6.

[1]State Key Laboratory of Drug Research, Shanghai Institute of Materia Medica, Chinese Academy of Sciences, Shanghai, China. [2]University of Chinese Academy of Sciences, Beijing, China. [3]Department of Pharmaceutics, Wuya College of Innovation, Shenyang Pharmaceutical University, Shenyang, China. [4]Zhongshan Institute for Drug Discovery, Shanghai Institute of Materia Medica, Chinese Academy of Sciences, Zhongshan, China.

Corresponding Authors: Likun Gong, Shanghai Institute of Materia Medica, Chinese Academy of Sciences, 501 Hai-ke Road, Shanghai 201203, China. E-mail: lkgong@simm.ac.cn; and Jianhua Sun, E-mail: jhsun@cdser.simm.ac.cn

Cancer Immunol Res 2023;11:241–60

doi: 10.1158/2326-6066.CIR-22-0439

Materials and Methods

Cells

Jurkat, RKO, CT26, B16F10, MC38, 4T1, Lewis lung carcinoma (LLC), Hepa1-6, YAC-1, HEK293T, and 293-AAV cell lines were purchased from Procell. The Pan02 cell line was purchased from BeNa. B16-F10, LLC, Hepa1-6, Pan02, HEK293T, and 293–adeno-associated virus (AAV) cells were cultured in Dulbecco's Modified Eagle Medium (DMEM; MA0212, Meilunbio) supplemented with 1% penicillin/streptomycin (P/S; 15140122, Invitrogen) and 10% heat-inactivated fetal bovine serum (FBS; 10100147, Life Technologies). Jurkat, CT26, MC38, YAC-1, and 4T1 were cultured in RPMI-1640 medium (MA0215, Meilunbio) containing 1% P/S and 10% FBS. RKO cells were cultured in minimum essential medium (MEM; MA0217, Meilunbio) supplemented with 1% P/S and 10% FBS. All cell lines were obtained from 2019 to 2022 and passed short tandem repeat analysis (Procell) and mycoplasma testing (40601ES20, Yeasen) before use. The number of cell passages was controlled within 15 passages. Other stable cell lines were constructed by the lentivirus system and cultured under the same conditions as the parental cells (see "Construction of stable cell lines"). Human peripheral blood mononuclear cells (PBMC) were purchased from Milestone (PB009C-1). All cells were cultured at 37°C in a 5% CO_2 humidified atmosphere.

Plasmids and viruses

All the plasmids were purchased from Youbio. pVSV-G (VT1470), pMDlg/pRRE (VT1449), and pRSV-Rev (VT1445) were used to package lentiviruses. pLKO.1-TRC (VT1413) was used to express shRNA. LentiCRISPRv2 (VT8107) was used to express sgRNA. pscAAV-ZsGreen1-shRNA (VT8093), pHelper (VT1800), and pAAV-RC (VT1521) were used to package self-complementary AAV serotype (scAAV). shRNA sequences: mouse CMTM6, 5′-TGCCTAACAGAAAGCGTGT-3′; mouse PD-L1, 5′-CCGAAATGATACACAATTCGA-3′; nontargeting, 5′-GGGTATCGACGATTACAAA-3′. sgRNA sequences: mouse CMTM6, 5′-CCTGGCCGCCTACTTCGTCC-3′; mouse PD-L1, 5′-GTATGGCAGCAACGTCACGA-3′; human CMTM6, 5′-CCGGGTCCTCCTCCGTAGTG-3′.

Mice

Female 6- to 8-week-old BALB/c and C57BL/6 mice were purchased from the Shanghai Slack. CMTM6$^{-/-}$, PD-L1$^{-/-}$, and PD-1$^{-/-}$ mice were purchased from GemPharmatech. Balb/c nu/nu mice were purchased from Vital River Laboratory. NSG mice were purchased from the Jackson Laboratory. CMTM6 and PD-L1 double-knockout mice were obtained by breeding CMTM6$^{-/-}$ and PD-L1$^{-/-}$ mice. All mice were maintained under specific pathogen-free conditions in the animal facility of the Shanghai Institute of Materia Medica, Chinese Academy of Sciences (SIMM). Animal care and experiments were performed in accordance with protocols approved by the Institutional Laboratory Animal Care and Use Committee (IACUC).

Construction of stable cell lines

All stable cell lines, including various CMTM6 or PD-L1 knockdown or knockout cell lines, were constructed using the lentiviral system. The corresponding shRNAs and sgRNAs are listed above (see "Plasmids and viruses"). Briefly, the gene of interest was subcloned into lentiviral expression vector (pLKO.1-TRC or LentiCRISPRv2; 3.5 μg), which was then transfected using Lipofectamine 3000 (L3000150; Thermo) into HEK293T cells (10 cm cell culture dish; 60% cell confluency) with the package plasmids (pVSV-G, pMDlg/pRRE, and pRSV-Rev; 3.5 μg/each). Three days later, the virosomes were collected by lentivirus concentration kit (GM-040801; Genomeditech) and inflected into HEK293T cells. The stable cells were obtained after antibiotic [puromycin (MA0318; Meilunbio) or hygromycin B (MA0210; Meilunbio)] resistance selection and were identified by Western Blot or flow cytometry.

Construction of scAAV

All scAAV-related vector construction, virus packaging, and titer identification were done by VectorBuilder Inc. The development of the scAAVs is described in the section "scAAV-mediated CMTM6 suppression is an effective tumor immunotherapy" in Results. Briefly, CMTM6 or PD-L1 targeting shRNAs were subcloned into pscAAV-ZsGreen1-shRNA vector and cotransfected into 293-AAV cells with packaging plasmids (pHelper and pAAV-RC). Three days later, cell supernatants were collected and concentrated by PEG to obtain virosomes.

TCGA analysis

Clinical pan-cancer *CMTM6* mRNA expression data were obtained from the TCGA data sets (https://portal.gdc.cancer.gov/) by GEPIA software. The number of tumor or normal samples is indicated in the figures. Expression differences, prognostic correlation, and immunologic correlation were analyzed by GEPIA software and R software v4.0.3.

Tumor models using transgenic tumor cells or transgenic mice

For all the subcutaneous models, mice were randomly grouped and injected subcutaneously with 5×10^5 tumor cells in the right forelimb. Tumor volume was measured and recorded every 2 or 3 days, except for Pan02 tumors (4 days). Tumor volume was calculated as tumor volume (mm^3) = tumor length × width × width/2, and tumor growth curves were plotted. At least 5 time points after tumor inoculation, the mice were sacrificed and the tumors were harvested for weighing, photographing, or other purposes. For survival studies, euthanasia endpoints were set as tumors larger than 2,000 mm^3 or larger than 20 mm in length or mice with significant weight loss. For the lung metastasis model, 1×10^6 B16F10 cells were injected into C57BL/6 mice or Balb/c nu/nu mice through the tail vein. After 20 days, the mice were sacrificed, and the lungs were harvested for weighing and photographing.

In vivo treatment studies

Studies of anti–CTLA-4 (BE0032, Bio X Cell) and anti–PD-L1 (BE0101, Bio X Cell) therapy in mice bearing 4T1 and LLC tumors, as well as studies of scAAV monotherapy and combination treatment, are consistent with the descriptions above. The administration methods of each drug are shown in the respective flow charts in the figures.

Immune cell depletion study

Mice were randomly divided and injected with tumor cells (CT26, B16F10, or MC38) subcutaneously, which was defined as day 0. $CD4^+$ T cells were deleted by intraperitoneal (i.p.) injection of anti-CD4 (BE0119, Bio X Cell) on day −2 (150 μg/each), day 0 (150 μg/each), day 4 (150 μg/each), and day 8 (150 μg/each). $CD8^+$ T cells were deleted by i.p. injection of anti-CD8β (BE0223, Bio X Cell) on day −2 (100 μg/each), day 0 (100 μg/each), day 4 (100 μg/each), and day 8 (100 μg/each). Natural killer (NK) cells of C57BL/6 mice were deleted by i.p. injection of anti-NK1.1 (BE0036, Bio X Cell) on day −2 (200 μg/each), day 0 (200 μg/each), day 4 (100 μg/each), and day 8 (100 μg/each). NK cells of BALB/c mice were deleted by i.p. injection

of anti-Asialo-GM1 (146002, BioLegend) on day −2 (35 μL/each), day 0 (35 μL/each), day 4 (35 μL/each), and day 8 (35 μL/each). Macrophages were deleted using chlorophosphate-liposomes (200 μL/each/ i.p. 40337ES08, Yeasen) on days −2, 4, and 8. $CD3^+$ T cells were deleted by FTY720 (MB1552, Meilunbio) on day −1 (30 μg/each), day 0 (30 μg/each), and days 1 to 12 (6 μg/each). The deletion effect was identified by flow cytometry (see "Immunophenotyping analysis").

Immunophenotype analysis

For immunotyping of intratumoral cells, tumor tissues were digested by collagenase IV (40510ES60, Yeasen) and hyaluronidase (20426ES60, Yeasen) and were filtered through 75-μm nylon mesh (7061011, Dakewe) into single-cell suspensions and then were subjected to cell extraction using lymphocyte separation medium (7211011, Dakewe) for sorting tumor-infiltrating lymphocytes (TIL) or were subjected to erythrocyte removal by red blood cell lysis buffer (40401ES60, Yeasen) for nonlymphocyte staining. Then, the cells were blocked with 4% FBS and anti-CD16/CD32 (553141, BD Biosciences), incubated with surface marker antibodies for 20 minutes at 4°C and then permeabilized with BD cytofix/cytoperm buffer (554714) before intracellular labeling antibodies were added for 30 minutes at 4°C. Then transcription factors were labeled for 45 minutes at 4°C by antibodies after being permeabilized with BD TF Fix/Perm buffer (562574). Flow cytometry analysis was performed using ACEA NovoCyte, and data processing was done through NovoExpress software (version 1.4.0). Antibody staining was performed following the manufacturer's recommendations. Please refer to Supplementary Table S1 for information about the antibodies used. For the immunotyping of splenocytes and thymocytes, single-cell suspensions were obtained by grinding tissues and were subject to erythrocyte removal. The other steps are the same as above.

In vitro cell assays

For analysis of dynamic changes in CMTM6 expression during activation of Jurkat cells, Jurkat cells were seeded in 24-well plates and stimulated with 50 ng/mL of PMA (MB5349, Meilunbio) and 1 μg/mL of ionomycin (MB7511, Meilunbio) for 0, 2, 6, 12, 24, and 48 hours, respectively. After fixation and permeabilization, the cells were stained with anti-CMTM6 (ab264067, Abcam) and goat anti-rabbit IgG H&L (Alexa Fluor 647; ab150079, Abcam) and detected by flow cytometry.

For the analysis of the effect of CMTM6 deficiency on PD-L1 expression in tumor cells, Cas9 control or CMTM6 knockout tumor cells (CT26, B16F10, MC38, or 4T1) were directly analyzed for PD-L1 expression (BV786 Rat Anti-Mouse CD274; 741014, BD Biosciences) by flow cytometry, or after being induced by 100 ng/mL of IFNγ (Z02916, GenScript) for 24 hours.

For the analysis of CMTM6 affecting Jurkat PD-L1, CMTM6-deficient Jurkat cells were constructed through the CRISPR/Cas9 system. PD-L1 levels were detected by flow cytometry 24 hours after Jurkat cells were stimulated with 50 ng/mL of PMA and 1 μg/mL of ionomycin.

For the cell proliferation assay, 1,000 tumor cells were seeded in 96-well plates. CCK8 (40203ES60, Yeasen) was added at 0, 24, 48, 72 hours, respectively, and the signal was read at OD 450 nm by an automatic microplate reader SpectraMax (Molecular Devices).

For signaling pathway protein detection in CT26 and B16F10 cells, phosphorylation indicators were detected by flow cytometry after fixation with Fixation Buffer (554655, BD Biosciences) and permeabilization with Perm Buffer III (558050, BD Biosciences), and nonphosphorylation indicators were detected by flow cytometry after treatment with Cytofix/Cytoperm Soln Kit.

Ex vivo cell assays

For the TIL–CT26 coculture study, 3×10^5 of CT26 cells were seeded in 24-well plates 12 hours in advance. TILs were isolated (see "Immunophenotyping analysis") and added to the wells at a ratio of 5:1 and 10:1, respectively. After 24 hours, TILs were removed by phosphate-buffered saline (PBS) washing, and the supernatant was used for cytokine detection by enzyme-linked immunosorbent assays (ELISAs) using the following kits for IFNγ (EM007-96, ExCell) and TNFα (EM008-96, ExCell). The cell viability of CT26 cells was analyzed by CCK8 assays (see "In vitro cell assays"). The survival of CT26 cells was analyzed by annexin V–FITC/PI apoptosis detection kit (40302ES20, Yeasen). CT26 cells (5×10^5) were stained with annexin V–FITC/PI at 25°C for 15 minutes. After being washed, annexin V–FITC and PI signals were detected by flow cytometry.

Wild-type or $CMTM6^{-/-}$ C57BL/6 mice were sacrificed, and the spleens and thymuses were collected for single-cell suspensions. Without stimulation, splenocytes and thymocytes were analyzed for preactivated phenotypes and cell development by flow cytometry using specific antibody staining (see Supplementary Table S1). Splenocytes (2×10^6) were added to 12-well plates and were stimulated with 50 ng/mL of PMA and 1 μg/mL of ionomycin for 24 hours for activation phenotype analysis or PD-L1 expression analysis, or for 0, 24, 48, 72, and 96 hours for dynamic change of CMTM6 expression analysis.

Freshly recovered human PBMCs (Milestone) were seeded at 5×10^5 of per well in 24-well plates. Without stimulation, CMTM6 expression of immune cell subsets in PBMCs was detected by flow cytometry. PBMCs were stimulated with 50 ng/mL of PMA and 1 μg/mL of ionomycin for 0, 24, 48, 72, and 96 hours. Subsequently, cell-surface expression of PD-1, PD-L1, and CMTM6 was measured by flow cytometry.

For NK-cell activation and killing assays, NK cells were isolated from mouse spleens by magnetic bead sorting (NK Cell Isolation Kit, mouse; 130-115-818, Miltenyi). 1×10^6 of NK cells were added to 24-well plates and were stimulated with 50 ng/mL of PMA and 1 μg/mL of ionomycin or 50 ng/mL IL2 (Z02764, GenScript) for 24 hours and were measured by flow cytometry for activation phenotype analysis. For the killing assays, 1×10^5 of YAC-1 cells were seeded in 96-well plates. NK cells were added to the wells at a ratio of 5:1 and 10:1, respectively. After 5 hours, the survival of YAC-1 cells was analyzed by the annexin V–FITC/PI apoptosis detection kit.

RKO/PBMC humanized tumor model

Female NSG mice were randomly divided into groups of 4. Frozen PBMCs (Milestone) derived from the same individual were revived in a 37°C water bath and used immediately. Mice were inoculated subcutaneously with RKO cells (5×10^6) mixed with human PBMCs (1×10^6) or RKO cells only on the right flank. Tumor volumes were monitored every 5 days for 5 time points.

Adoptive transfusion of immune cells

For the adoptive transfusion of TILs, donor mice were inoculated with CT26 tumor cells (5×10^5) 6 days before the recipient mice. On day 6 of tumor growth in recipient mice, the donor mice were sacrificed and tumor tissue was obtained. Under aseptic conditions, TILs were isolated. TILs (5×10^6) were peritumorally injected into recipient mice. For splenocyte and T-cell transfusion, under aseptic

conditions, spleens from C57BL/6 mice were processed as described above, and the T cells were obtained by magnetic bead sorting (Pan T Cell Isolation Kit II; 130-095-130, Miltenyi). Splenocytes or T cells (5×10^6) were peritumorally injected into recipient mice with tumor growth for 7 or 10 days. Tumor growth kinetics, volumes, and weights were measured.

Analysis of scAAV infection

In vitro, 1×10^5 of CT26 and B16F10 cells were inoculated in 24-well plates, respectively. After 8 hours, scAAV was added to the well plates at an MOI of 10,000. After 72 hours of infection, the green fluorescent signal was detected by flow cytometry and fluorescence microscopy (Echo). *In vivo*, 5×10^9 of scAAV were peritumorally injected at day 6 of tumor growth. After 3 days, the tumor tissues were collected and processed into single-cell suspensions, and the green fluorescence signal in each cell subpopulation was analyzed by immunotyping.

Single-cell sequencing data analysis

Single-cell RNA sequencing (RNA-seq) data used in this study were all from publicly available data. Data for CMTM6 expression in immune cells were obtained from the GEO database (GSE127465) and the Human Protein Atlas Project (https://www.proteinatlas.org/). The SpringViewer interactive tool was used to analyze the data. Data for CMTM6 expression in tumor-infiltrating T cells were obtained from the GEO database (GSE156728) and analyzed by the scDVA interactive tool (http://cancer-pku.cn:3838/PanC_T/).

RNA-seq

About 30 mg of fresh tumor tissues were obtained from sacrificed CT26 or B16F10 tumor-bearing mice. RNA isolation, transcriptome libraries construction, sequencing, and basic data analysis were conducted by BGI. Based on the RNA-seq raw data, differential expression was evaluated with DESeq. A fold change of 2:1 or greater and a false discovery rate (FDR)-corrected *P* value of 0.05 or less were set as the threshold for differential genes. Immune signature scores are defined as the mean $\log_2$(fold-change) among all genes in each gene signature list from gene set enrichment analysis data sets. Cell infiltration within tumor tissues was estimated by xCell (https://xcell.ucsf.edu/).

Statistical analysis

The *in vivo* experiments were randomized but the researchers were not blinded to allocation during experiments and outcome analysis. Statistical analysis was performed using GraphPad Prism 8 Software. A Student *t* test was used for comparison between the two groups. Multiple comparisons were performed using one-way ANOVA followed by Tukey multiple comparisons test or two-way ANOVA followed by the Tukey multiple comparisons test. Survival analysis was performed by the Kaplan–Meier method. Detailed statistical methods and sample sizes in the experiments are described in each figure legend. No statistical methods were used to predetermine the sample size. All statistical tests were two-sided, and *P* values < 0.05 were considered to be significant. Ns, not significant; *, $P < 0.05$; **, $P < 0.01$; ***, $P < 0.001$.

Data and materials availability

All data are available in the main text or the supplementary materials or are available upon request from the corresponding author. Correspondence and requests for materials should be addressed to L. Gong.

Results

The association of CMTM6 expression with clinical malignancies

To determine whether there is a correlation between CMTM6 expression and clinical malignancy progression, we first analyzed differences in the expression of CMTM6 between 33 cancers and normal tissues using the GEPIA tool (43) based on TCGA data sets and found that CMTM6 expression was significantly elevated in 10 cancers (**Fig. 1A**), including colon adenocarcinoma and pancreatic adenocarcinoma (PAAD). Numerous other cancers showed elevated CMTM6 expression trends. Then, the relationship between OS and CMTM6 expression was analyzed for the same 33 cancers in the TCGA data sets, and high CMTM6 levels in three cancers, adrenocortical carcinoma (ACC), brain lower grade glioma (LGG), and PAAD, were found to significantly associate with poorer patient prognosis (Supplementary Fig. S1).

CMTM6 deficiency reduces murine tumor growth and metastasis *in vivo*

Next, to assess the effects of CMTM6 on tumor growth, we knocked out the *Cmtm6* gene in six murine cancer cell lines (CT26, B16F10, 4T1, LLC, Hepa1-6, and MC38), representing five tumor types, using the CRISPR–Cas9 system (Supplementary Fig. S2A). Using wound healing and proliferation assays, knocking out CMTM6 was found to not significantly alter the *in vitro* growth and migration rates of tumor cells (Supplementary Fig. S2B–S2I). Consistent with earlier studies, CMTM6 deficiency significantly reduced cell-surface PD-L1 expression in several murine cancer cell lines in the presence or absence of IFNγ induction (Supplementary Fig. S3). For the colorectal cancer cell line CT26, shRNA-mediated knockdown of CMTM6 showed a significant tumor-suppressive effect *in vivo*, with a 73.0% inhibition rate (IR) compared with the control group (**Fig. 1B**). This suppression of tumor growth was comparable with that seen for PD-L1 knockdown (IR: 70.01%). Similarly, when CMTM6 knockout cells, including the colorectal cancer cell lines CT26 and MC38, the melanoma cell line B16F10, the HCC cell line Hepa1-6, and the NSCLC cell line LLC, were inoculated into syngeneic mouse hosts, their abilities to form tumors were significantly attenuated compared with vector controls (**Fig. 1C–G**). Moreover, mouse recipients of CMTM6 knockout cells showed prolonged survival (**Fig. 1H** and **I**). In addition, tumor CMTM6 deficiency inhibited tumor metastasis in a B16F10 lung metastasis model (**Fig. 1J**).

CMTM6 expression increases with tumor progression

Flow-cytometric analysis of changes in CMTM6 expression *in vivo* showed that CMTM6 expression levels were 40.1% higher in 14-day B16F10 melanoma cells than in 7-day cells (**Fig. 1K**). We then analyzed the clinical grading information available in the TCGA data sets for the aforementioned three cancers associated with patient prognosis (ACC, LGG, and PAAD) and found that all three cancers showed escalating CMTM6 expression with clinical disease progression, particularly LGG and PAAD (Supplementary Fig. S4A–S4C). Considering the clinical refractoriness of pancreatic cancer, we constructed a CMTM6 knockout mouse pancreatic tumor cell line, Pan02 (Supplementary Fig. S4D). CMTM6 deficiency significantly inhibited the growth of Pan02 tumors *in vivo* (Supplementary Fig. S4E), which reinforces the potential clinical value of targeting CMTM6 in pancreatic cancer.

The above data illustrate that CMTM6 levels correlate with tumor progression and patient prognosis in clinical samples and mouse models. In pan-cancer, lowering CMTM6 in tumor cells effectively impedes tumor growth and metastasis *in vivo*.

Correlation between CMTM6 expression and the immunophenotype of clinical tumors

To further assess the impacts of CMTM6 on human tumor growth, we knocked out the *CMTM6* gene in the human colorectal cancer cell line RKO using the CRISPR–Cas9 system (Supplementary Fig. S5A; **Fig. 2A**). In a humanized mouse model, ablation of CMTM6 significantly inhibited RKO tumor growth *in vivo* (**Fig. 2A**). This phenomenon was not observed in highly immunodeficient NSG mice that did not receive PBMC coinjection, implying a connection between the effect of CMTM6 on oncogenesis and the immune system. Therefore, we investigated whether there was a correlation between CMTM6 expression and immune cell infiltration in human tumors by analyzing the TCGA data sets using the TIMER tool (44) and found that expression of CMTM6 was positively correlated with infiltration of T helper 2 cells (Th2) and regulatory T cells (Treg), and negatively correlated with the infiltration of $CD8^+$ T cells, Th1, and natural killer T cells (NKT; **Fig. 2B**). Moreover, in TCGA tumors with high CMTM6 expression, CMTM6 expression was significantly positively correlated with expression of PD-L1, T-cell immunoglobulin mucin-3 (TIM-3), B7-H3, and other immune checkpoints (Supplementary Fig. S5B–S5D). In addition, data from several genome-wide CRISPR library screenings (45–47) suggested that CMTM6 knockout in murine tumor cells promoted CTL killing to varying degrees (**Fig. 2C**). These data emphasize the relationship between host immunity, particularly T-cell immunity, and CMTM6 function.

CMTM6 deficiency can reverse immune-checkpoint inhibitor resistance

We next tested whether CMTM6 knockout would affect the efficacy of ICB therapy using anti–PD-L1–resistant 4T1 tumors and anti–PD-L1–resistant and anti–CTLA-4–resistant LLC tumors. The results showed that CMTM6 knockout could restrain both tumors' growth, and CMTM6-deficient tumors could respond to anti–PD-L1 and anti–CTLA-4 (**Fig. 2D** and **E**). Anti–PD-L1 inhibited CMTM6-deficient 4T1 with an IR of 43.4%. Anti–PD-L1 and anti–CTLA-4 inhibited CMTM6-deficient LLC with IR of 48.5% and 47.4%, respectively. These data suggest that tumor CMTM6 deficiency can reverse ICB resistance.

Inhibition of tumor growth by CMTM6 deficiency requires host immunity

To further investigate the involvement of host immunity, we inoculated CMTM6-deficient and Cas9 control B16F10, CT26, and 4T1 tumor cells into NSG mice or Balb/c nu/nu mice (**Fig. 2F–K**). Results showed that CMTM6-deficient cells showed no inhibition of tumor growth in NSG mice. Furthermore, CMTM6-deficient B16F10, CT26, and 4T1 tumor cells formed tumors in Balb/c nu/nu mice deficient in T cells as efficiently as appropriate control tumor cells. In addition, the effect of CMTM6 deficiency on B16F10 tumor lung metastasis also disappeared in Balb/c nu/nu mice (**Fig. 2L**). These data suggest that host immunity, especially T-cell immunity, plays a decisive role in tumor suppression caused by CMTM6 deficiency.

CMTM6 deficiency promotes antitumor cytotoxicity

We next systematically investigated the involvement of host immunity in CMTM6 function. We first carried out a lymphocyte adoptive transfusion experiment using TILs from CMTM6 KO and Cas9 control CT26 tumors (**Fig. 3A**). CCK8 assays showed that TILs of CMTM6 KO tumors had higher cell viability both at isolation and after 24 hours of *in vitro* culture (Supplementary Fig. S6A and S6B). The TILs were then transfused into CT26 tumors. The results showed that compared with the PBS group, infusion of TILs from Cas9 control tumors promoted tumor growth, whereas infusion of TILs from CMTM6 KO tumors hampered tumor growth (**Fig. 3B**). Tumor volume and weight in the former group were more than twice as large as those in the latter group. In addition, when isolated TILs and CT26 cells were cocultured *in vitro*, TILs from CMTM6 KO tumors triggered significantly greater apoptosis of CT26 cells and significantly greater specific cytokine production compared with the Cas9 control tumors' TILs (**Fig. 3C**; Supplementary Fig. S6C–S6E). TILs from Cas9 control tumors were unable to produce IFNγ when cocultured with CT26 cells, whereas TILs from CMTM6 tumors produced high levels of IFNγ when cocultured with CT26 (Supplementary Fig. S6D).

We next attempted to quantify the immune effector cells in shNC, shCMTM6, and shPD-L1 CT26 tumors by flow cytometry (Supplementary Figs. S7 and S8A). Immunophenotyping demonstrated that shRNA-mediated knockdown of tumor CMTM6 considerably promoted the effects of intratumoral cytotoxic cells, including NK cells, NKT cells, and $CD8^+$ T cells, significantly increased Th1 infiltration and reduced Th17 infiltration (**Fig. 3D**). The proportion of $FasL^+$, granzyme B^+, $perforin^+$, and $TNF\alpha^+$ cytotoxic cells was increased in shCMTM6 tumors. Increased expression of some checkpoint molecules on effector cells may be due to higher activation levels of the immune system. Significant reductions in intratumoral $PD\text{-}L1^+$ myeloid cell subsets and $PD\text{-}L1^+$ tumor cells were observed (Supplementary Fig. S8B). Similar immunophenotyping results were identified in CMTM6-knockout "cold" 4T1 tumors, suggesting that tumor CMTM6 deficiency can remodel the tumor microenvironment (TME) (Supplementary Fig. S9). Tumor CMTM6 suppression substantially improved intratumoral NK-cell function more than tumor PD-L1 suppression, suggesting the existence of certain differences in the regulation of the TME by the two molecules (**Fig. 3D**).

To determine the relative importance of different immune effector cells, we conducted a series of immune cell depletion experiments. The pivotal role of T-cell immunity in the involvement of CMTM6 in tumor immunity was by the loss of tumor growth inhibition in the presence of FTY720, which inhibited intratumoral indicated infiltration of T cells (**Fig. 3E**). We then found that $CD8^+$ T cells and NK cells played a dominant role in suppression of tumor growth induced by CMTM6 knockout in CT26 and MC38 tumors (**Fig. 3F** and **G**). Deletion of $CD8^+$ T cells resulted in no significant difference in weight between CMTM6 KO and Cas9 control tumors in both models. The involvement of $CD4^+$ T cells and macrophages did not seem to matter, especially macrophages.

RNA-seq analysis of the effect of CMTM6 knockout in B16F10 and CMTM6 knockdown in CT26 on the complex TME showed that tumor CMTM6 deficiency affected multiple immune processes in both models, especially the adaptive immune process, interferon process, T-cell function, and NK-cell function (**Fig. 3H**; Supplementary Fig. S10). In addition, xCell analysis of sequencing data showed that, consistent with the above results, infiltration of $CD8^+$ T cells and NK cells was significantly increased in shCMTM6 tumors (**Fig. 3I**). We also observed that platelets, pericytes, microvascular endothelial cells, and other tumor angiogenesis–related cells decreased significantly.

Taken together, these results suggest that tumor CMTM6 deficiency remodels the TME and mobilizes antitumor effector cells. Intratumoral cytotoxic cells and their specific tumor-killing effects mainly contribute to tumor suppression mediated by CMTM6 deficiency.

CMTM6 deficiency inhibits tumor growth in the absence of the PD-1/PD-L1 axis

Studies have established that CMTM6 can affect PD-L1 stability on tumor cell membranes (8, 9), and our work also found that suppression of CMTM6 levels has similar effects on tumor immunity to PD-L1 inhibition. However, our results showed that although CMTM6 deficiency reduced membrane PD-L1 by less than half (Supplementary Fig. S3), the tumor inhibition effect was comparable with that of PD-L1 inhibition (**Fig. 1B**), suggesting that CMTM6 may be involved in tumor immunity not only through modulation of PD-L1. In addition, tumor CMTM6 suppression and PD-L1 suppression were not fully consistent in the regulation of the intratumoral immune

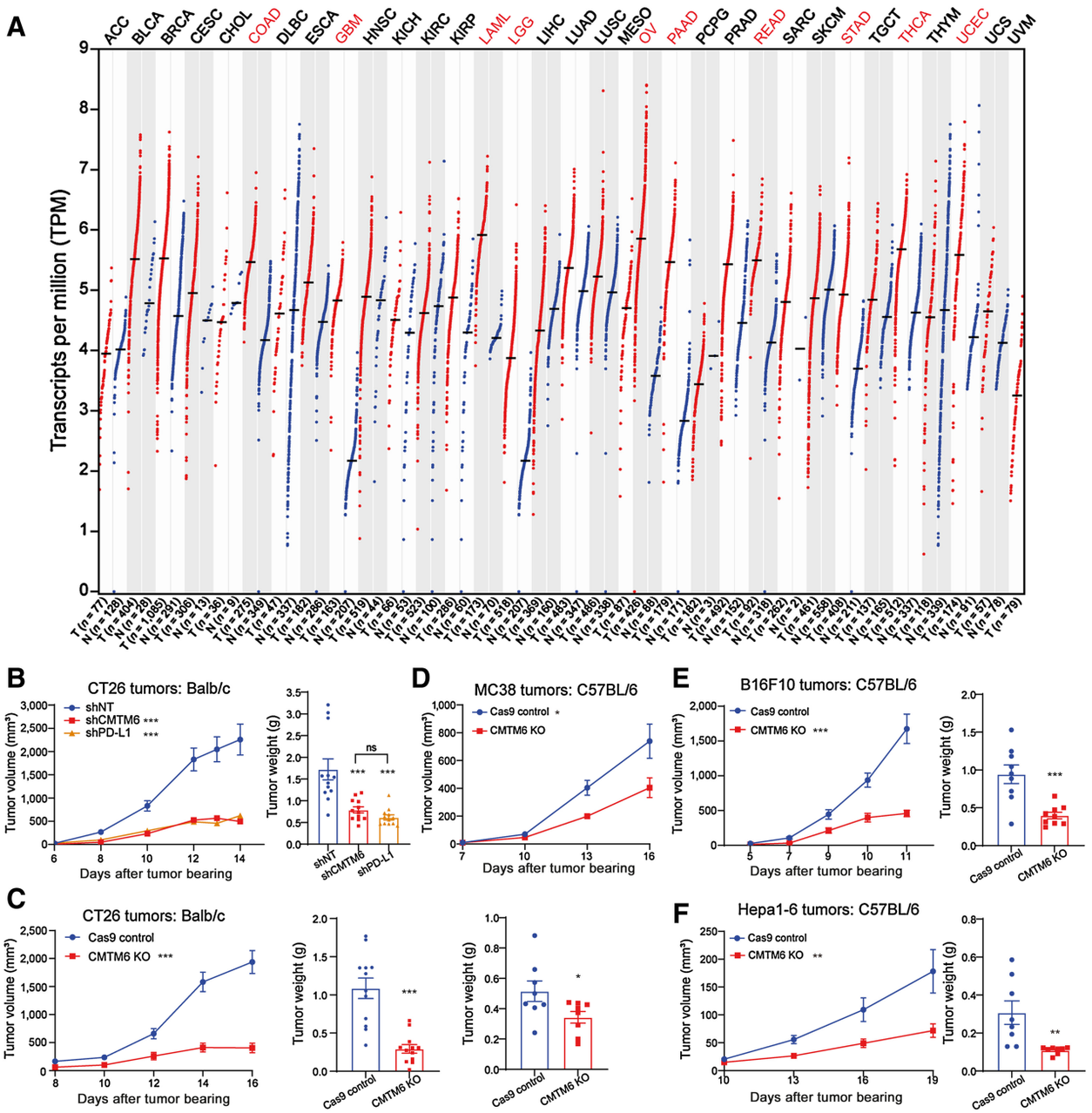

Figure 1.

CMTM6 suppression attenuated tumor growth in syngeneic mice. **A,** Human *CMTM6* mRNA levels in different tumor types from the TCGA database were compared with normal tissue *CMTM6* expression and were determined by GEPIA. The red font shows the tumors with a statistically significant difference in comparison with the Wilcoxon test. **B,** Tumor growth kinetics (left) and weights (right) of CT26 cells expressing CMTM6-shRNA (shCMTM6), PD-L1–shRNA (shPD-L1), or nontargeting shRNA(shNT) in Balb/c mice ($n = 12$). **C,** Tumor growth kinetics (left) and weights (right) of CT26 cells with CMTM6-sgRNA versus Cas9-control in Balb/c mice ($n = 12$). **D–G,** Tumor growth kinetics and weights of MC38 cells (**D**), B16F10 cells (**E**), Hepa1-6 cells (**F**), and LLC cells (**G**) with CMTM6-sgRNA versus Cas9-control in C57BL/6 mice ($n = 8$). (*Continued on the following page.*)

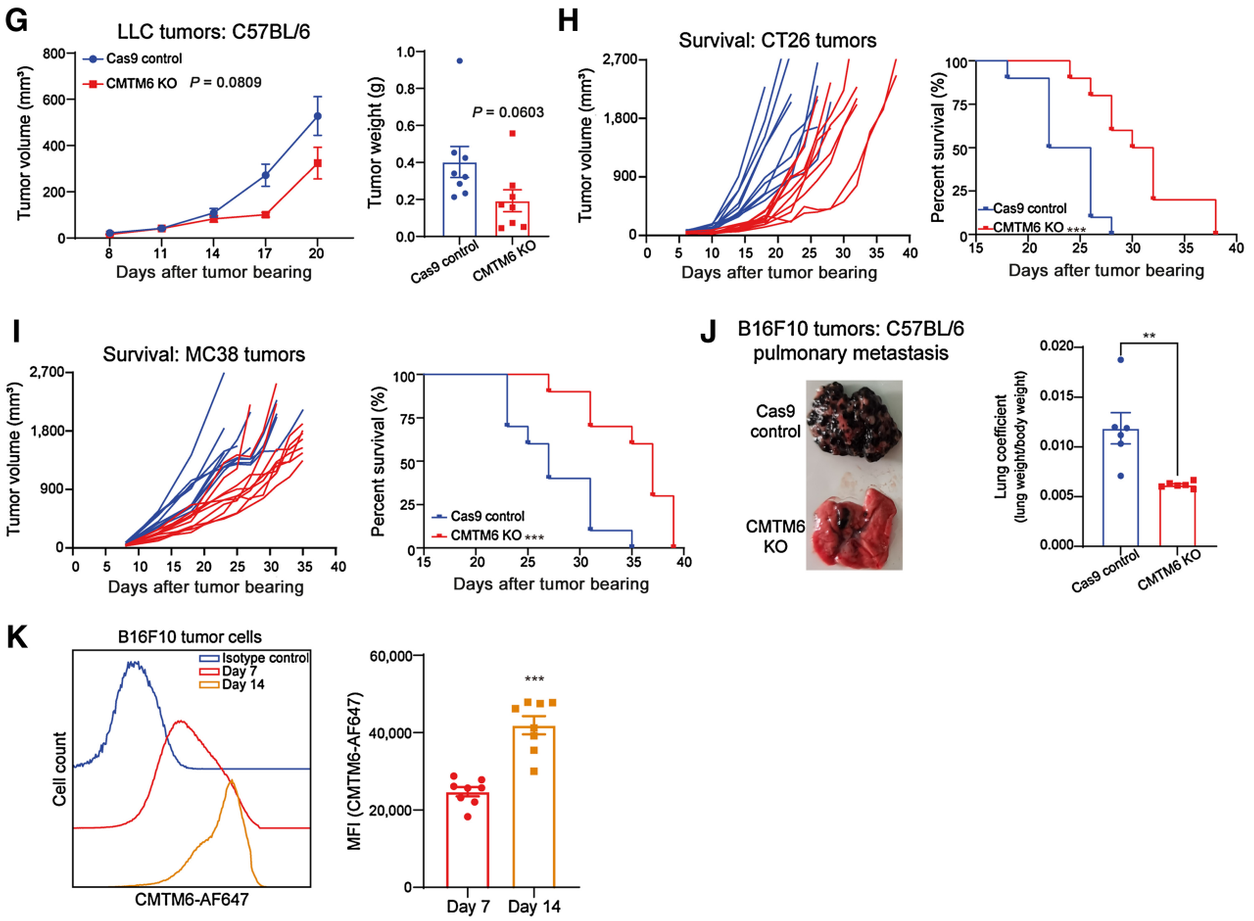

Figure 1.

(*Continued.*) **H,** Individual growth curves are shown for Cas9 control and CMTM6 KO CT26 tumors ($n = 10$; left). Right, Kaplan–Meier plot of survival. **I,** Individual growth curves are shown for Cas9 control and CMTM6 KO MC38 tumors ($n = 10$). Right, Kaplan–Meier plot of survival. **J,** A representative photograph of the whole lung is shown for pulmonary metastasis of Cas9 control and CMTM6 KO B16F10 tumors ($n = 6$). Right is the scatter plot of the lung coefficient (lung weight/body weight) for the two groups. **K,** Representative histograms show CMTM6 expression levels of B16F10 tumor cells measured by flow cytometry on day 7 and day 14 after tumor cells were administered to C57BL/6 mice. Right, scatter plot of median fluorescence intensity (MFI) for CMTM6 in two groups ($n = 8$). The data are presented as the mean ± SEM. *, $P < 0.05$; **, $P < 0.01$; ***, $P < 0.001$; ns, not significant by an unpaired *t* test or one-way ANOVA followed by Tukey multiple comparisons test. *P* values of survival plots were calculated by the log-rank test.

environment. Hence, we investigated the biofunction of CMTM6 in PD-L1$^{-/-}$ tumors.

Using wound-healing and proliferation assays, knocking out CMTM6 was found to not significantly alter the *in vitro* growth and migration rates of PD-L1 KO tumor cells (Supplementary Fig. S11). When PD-L1/CMTM6 double-knockout CT26 cells were inoculated into syngeneic mouse hosts, their capacity to form tumors was significantly attenuated compared with that of PD-L1 KO and CMTM6 KO tumors (**Fig. 4A**). Moreover, 100% tumor regression was achieved in CT26 tumors of mice in the PD-L1/CMTM6 KO group. Two weeks later, the 10 surviving mice were rechallenged with parental CT26 cells and monitored for tumor growth (**Fig. 4B**). Results showed that 7 of the 10 surviving mice rechallenged with CT26 tumors achieved complete regression, and the weight of tumors in the 3 other mice was significantly lower than that of the control group, suggesting that PD-L1/CMTM6 KO CT26 cells induced antitumor immune memory (**Fig. 4C**). Similarly, PD-L1/CMTM6 KO B16F10 tumors were significantly limited in growth compared with PD-L1 KO B16F10 tumors (**Fig. 4D**). Furthermore, in the MC38 model deletion of tumor CMTM6 inhibited tumor growth in WT C57BL/6 mice, whereas PD-L1 deletion did not (**Fig. 4E**). Moreover, in PD-1$^{-/-}$ mice, CMTM6 KO MC38 tumors were still limited in growth, and the tumor IR (40.9%) was the same as in WT mice.

Subsequently, in Balb/c nu/nu mice, PD-L1/CMTM6 KO did not significantly inhibit the growth of CT26 tumors compared with PD-L1 KO, and the inhibitory effect of PD-L1/CMTM6 KO was also greatly reduced in B16-F10 tumors compared with WT mice (**Fig. 4F** and **G**). In addition, by depleting CD8$^+$ T cells and NK cells from WT mice, we found that in the case of PD-L1 deficiency, the tumor suppression effect of CMTM6 deletion remained mostly dependent on CD8$^+$ T cells and NK cells, especially CD8$^+$ T cells (**Fig. 4H** and **I**).

The above results indicate that tumor CMTM6 can mediate tumorigenesis regulation independently of tumor PD-L1, and even the inhibitory effect of tumor CMTM6 ablation on tumor growth is largely unrelated to the PD-1/PD-L1 axis. The tumor immunomodulatory

effects of CMTM6 separated from modulation of PD-L1 remain largely cytotoxic-cell dependent.

CMTM6 affected β-catenin/CCL4 signaling in tumor cells independently of PD-L1

Considering that CMTM6 has been reported to be involved in regulating the Wnt signaling (34), we tested whether tumor CMTM6 KO affected the expression and activation of key molecules in the pathway independently of PD-L1 (Supplementary Fig. S12). In comparison with PD-L1–deficient CT26 cells, pS473-Akt, pS9-GSK3β, β-catenin, and nonphosphorylated active β-catenin expression levels were lower in CT26 cells with CMTM6/PD-L1 double KO. The same phenomenon was also observed in B16F10 cells, which suggested that independently of PD-L1, tumor CMTM6 KO could inhibit the activation of Akt, thereby reducing the inhibition of GSK3β and β-catenin activation. β-Catenin can

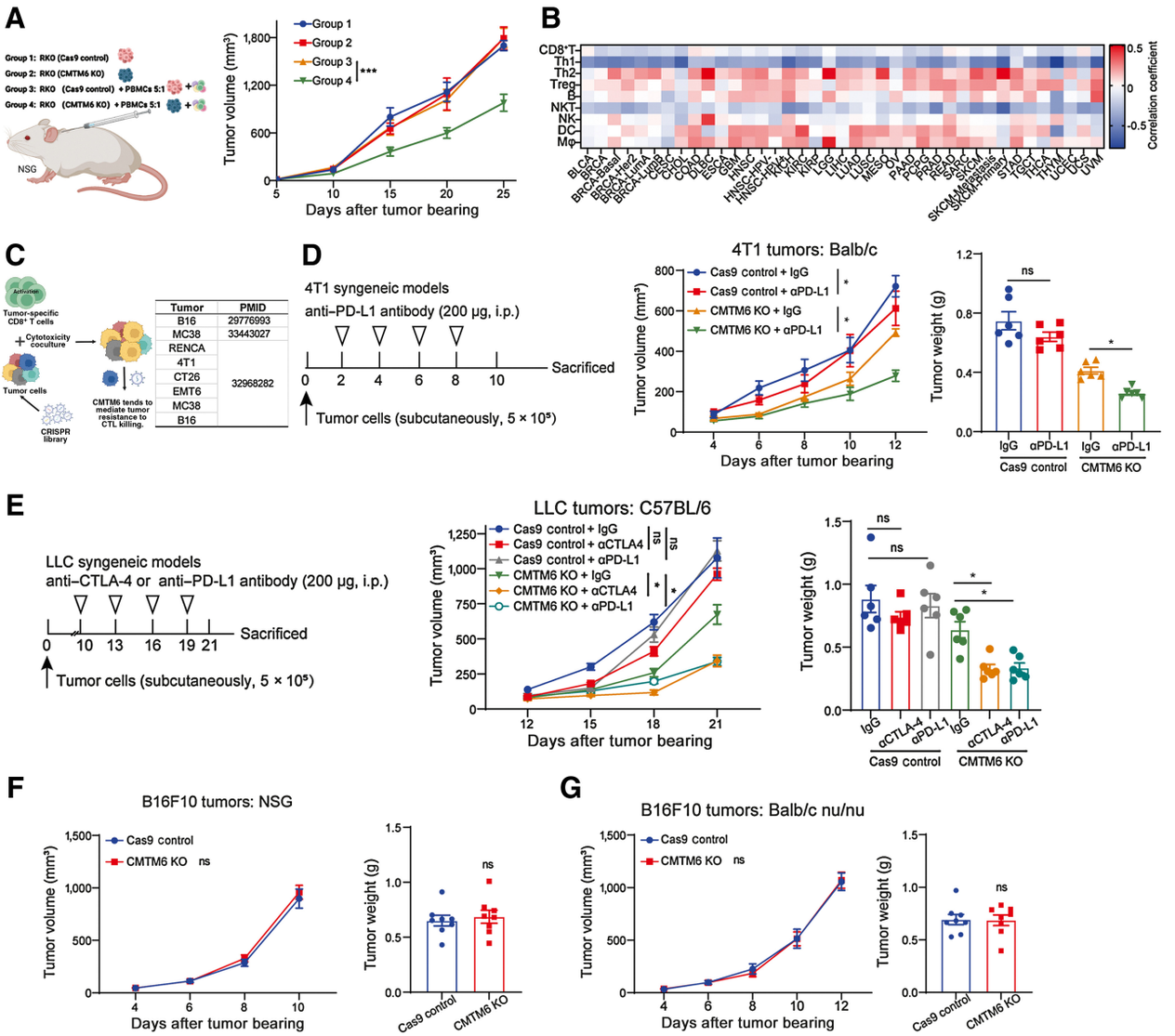

Figure 2.

Suppression of CMTM6 overcame tumor resistance to ICB and attenuated tumor growth dependent on the host immunity. **A,** Schematic diagram of the grouping of Cas9 control and CMTM6 KO human RKO tumor cells with or without mixed injection of human PBMCs. Tumor growth kinetics of four groups in NSG mice are shown ($n = 8$). **B,** The heat map shows the correlation of CMTM6 expression with immune cell infiltration level in different tumor types as indicated in the TCGA database and was determined by TIMER2.0. **C,** Schematic diagram of CRISPR library screening data reported in the literature shows CMTM6 deficiency in several murine tumor cells promotes killing by CTLs. **D,** Schematic of treatment schedules and dosing of anti–PD-L1 or isotype control against Cas9 control and CMTM6 KO 4T1 tumors in Balb/c mice ($n = 6$; left). Middle, graph of tumor growth curves; right, scatter plot of tumor weight. **E,** Schematic of treatment schedules and dosing of anti–PD-L1 and anti–CTLA-4 against Cas9 control and CMTM6 KO LLC tumors in C57BL/6 mice (left; $n = 6$). Middle, graph of tumor growth curves; right, scatter plot of tumor weight. **F–K,** Tumor growth kinetics and weights of CMTM6-sgRNA versus Cas9-control B16F10, CT26, and 4T1 cells in NSG mice ($n = 8$; **F, H, J**) or Balb/c nu/nu mice ($n = 8$; **G, I, K**). (*Continued on the following page.*)

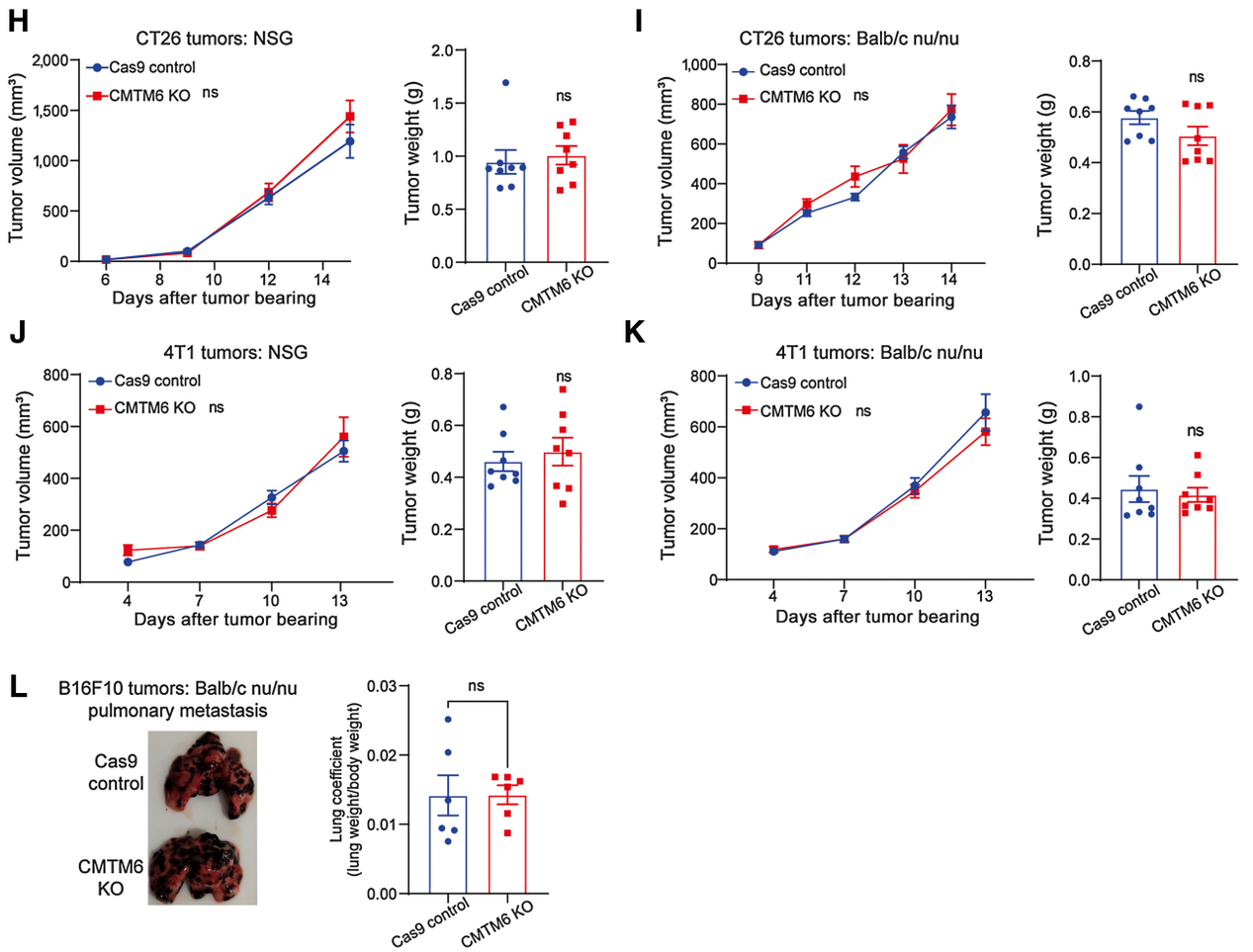

Figure 2.

(*Continued.*) **L,** A representative photograph of the whole lung is shown for pulmonary metastasis of Cas9 control and CMTM6 KO B16F10 tumors in Balb/c nu/nu mice ($n = 6$). Below is the scatter plot of the lung coefficient for two groups. Data, mean ± SEM. *, $P < 0.05$; ***, $P < 0.001$; ns, not significant by an unpaired *t* test or one-way ANOVA followed by the Tukey multiple comparisons test.

engage tumor immunity by regulating tumor CCL4 and CD47 expression (48–50). In CT26 and B16F10 cells, we found that tumor CMTM6/PD-L1 double KO increased the expression of CCL4 but not CD47 compared with PD-L1 KO. Considering that CCL4 mainly affects the intratumoral infiltration of $CD8^+$ T cells whereas CD47 is the phagocytosis checkpoint, these experimental results are consistent with the conclusions drawn from our immune cell depletion assays. Therefore, we speculated that independent of PD-L1, tumor CMTM6 KO could inhibit β-catenin levels and activation by affecting Akt/GSK3β/β-catenin signaling, thereby increasing tumor expression of CCL4 and recruiting more $CD8^+$ T-cell infiltration.

Host immune cell expression profile of CMTM6

Given that nontumor cells may also express tumor-regulatory molecules, we further evaluated CMTM6 expression and function in host cells. Through searching the Human Protein Atlas database (51), we found that under normal physiologic conditions, CMTM6 was widely expressed at the protein level in most human tissues (**Fig. 5A**). This was significantly different from the expression profile of PD-L1, which was detected only in few tissues such as the lung and colon (Supplementary Fig. S13). At the single-cell level (52, 53), CMTM6 was found to be preferentially expressed in granulocytes, monocytes, and macrophages both in immune organs and nonimmune organs such as the liver and lung (Supplementary Fig. S14). CMTM6 also was observed to be expressed in T cells, B cells, and NK cells (**Fig. 5B**; Supplementary Fig. S14). In addition, CMTM6 was expressed abundantly in somatic cells, especially hepatocytes (Supplementary Fig. S14). Although PD-L1 was also highly expressed in granulocytes and monocytes/macrophages, its overall single-cell expression profile was significantly distinct from that of CMTM6, and its expression level in the resting state was much lower than that of CMTM6 (Supplementary Figs. S13 and S14). A similar phenomenon was confirmed in single-cell sequencing data of mouse immune cells (**Fig. 5C**). We then analyzed mouse splenocytes and human PBMCs by flow cytometry and confirmed that CMTM6 was broadly expressed in immune cell subsets at the protein level (**Fig. 5D** and **E**).

CMTM6 expression changes dynamically with T-cell activation

Considering that T cell–intrinsic PD-L1 was recently found to play a nonnegligible role in tumor progression (54), we selected T-cell CMTM6 as the main research focus to explore the association between CMTM6 and PD-L1 on host T cells. First, in PMA and ionomycin-activated Jurkat human T cells, CMTM6 expression rose progressively during the stimulation (**Fig. 5F**). Following 48 hours of stimulation, CMTM6 levels were approximately 3 times higher than in the resting state. Similarly, upon stimulation of human PBMCs with PMA and ionomycin, CMTM6 expression on $CD3^+$ T cells increased, with a plateau obtained at around 96 hours after stimulation (**Fig. 5G**). PD-1 and PD-L1 expression on T cells were also increased with increased activation time (**Fig. 5H**). Moreover, coexpression of PD-1 and CMTM6 as well as PD-L1 and CMTM6 increased gradually with increasing activation time (**Fig. 5H**). After 48 hours of stimulation, more than 80% of T cells coexpressed CMTM6 and PD-1/PD-L1 molecules.

CMTM6 deficiency reduces membranal PD-L1 expression on T cells

To assess whether suppression of T-cell CMTM6 would also downregulate membranal PD-L1 on T cells, we analyzed CMTM6-deficient Jurkat cells (**Fig. 5I**). Membranal PD-L1 was significantly reduced in CMTM6 KO Jurkat cells compared with Cas9 control Jurkat cells 24 hours after PMA and ionomycin stimulation (**Fig. 5I**). Further, we isolated $CD3^+$ T cells from the spleens of $CMTM6^{-/-}$ mice and stimulated them with PMA and ionomycin for 24 hours. Compared with splenic T cells from WT mice, lower PD-L1 was found in CMTM6 KO splenic T cells (**Fig. 5J**). Specifically, CMTM6 deficiency reduced PD-L1 expression in activated mouse $CD4^+$ T and $CD8^+$ T cells by 34.7% and 42.9%, respectively (**Fig. 5K**). Moreover, CMTM6 deficiency did not affect PD-1 expression on activated $CD4^+$ T and $CD8^+$ T cells. Hence, T cell–intrinsic CMTM6 can also specifically affect the stability of PD-L1 on T-cell membranes.

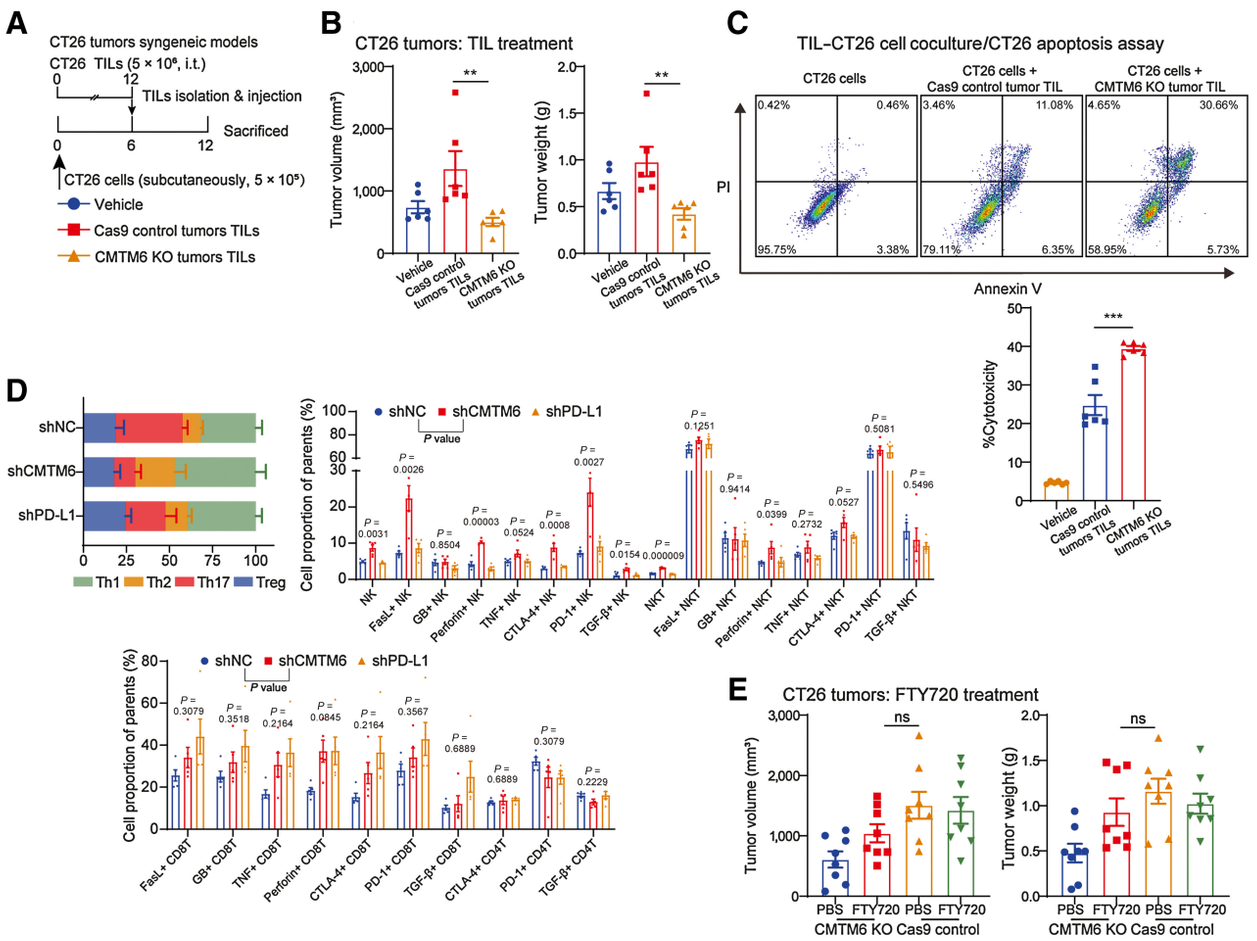

Figure 3.

Suppression of CMTM6 enhanced intratumoral antitumor cytotoxic immune responses. **A,** Schematic of TIL adoptive transfusion schedules. TILs isolated from Cas9 control and CMTM6 KO CT26 tumors were peritumorally injected into CT26 tumors. **B,** The volume and weight of CT26 tumors in Balb/c mice injected with adoptive TILs are shown ($n = 6$). **C,** CT26 cells and TILs were cocultured at a 5:1 ratio for 24 hours. Representative density plots and scatter plot show the viability of CT26 cells in the different coculture groups ($n = 6$). **D,** At 12 days after tumor administration, immune effector cells in shNC, shCMTM6, and shPD-L1 CT26 tumors were quantified by flow cytometry ($n = 5$). The percentages of specific $CD4^+$ T cells, $CD8^+$ T cells, and NK cells are shown based on their respective markers. **E,** Mice bearing Cas9 control or CMTM6 KO CT26 tumors were dosed with FTY720 or PBS as control. Tumor volume and weight are shown ($n = 6$). (*Continued on the following page.*)

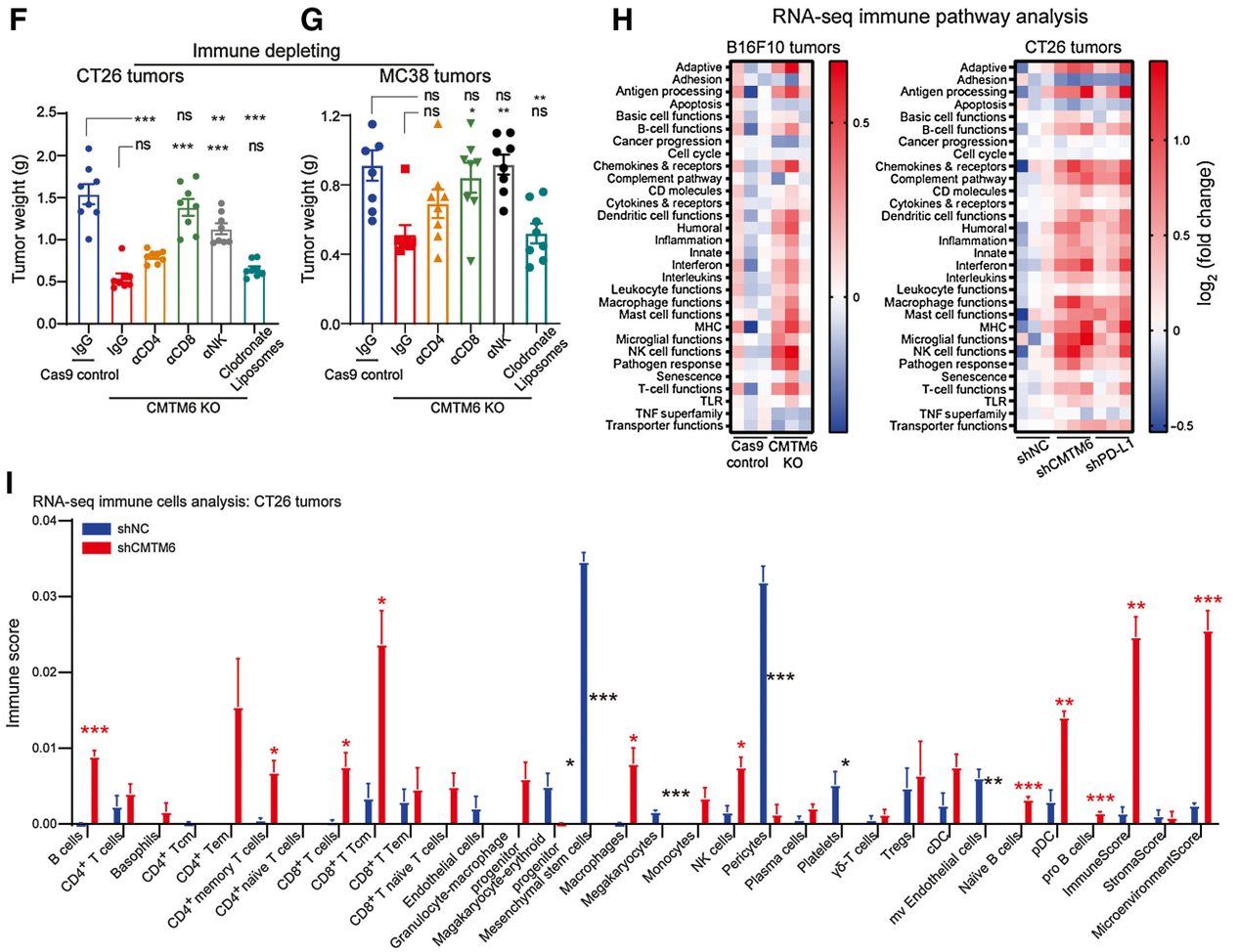

Figure 3.

(*Continued.*) **F,** Mice bearing Cas9 control and CMTM6 KO CT26 and MC38 tumors were dosed with the indicated immune cell depletion reagents. Tumor volume is shown ($n = 8$). **H,** Signature scores [defined as the mean $\log_2$(fold change) among all genes measured by RNA-seq in the signature] for immune-associated processes are shown as heat map ($n = 3$). **I,** Immune cell infiltration analysis by xCell for RNA-seq data ($n = 3$). The data are presented as the mean ± SEM. *, $P < 0.05$; **, $P < 0.01$; ***, $P < 0.001$; ns, not significant by an unpaired *t* test or one-way/two-way ANOVA followed by the Tukey multiple comparisons test.

CMTM6 deficiency and T-cell development and activation

By analyzing the proportion of $CD4^-CD8^-$ double-negative (DN) T cells, $CD4^-CD8^+$ T cells, $CD4^+CD8^+$ T cells, and $CD4^+CD8^-$ T cells in the thymus of CMTM6-deficient mice and the coexpression of CD44 and CD25 in the DN T cells, we preliminarily concluded that CMTM6 knockout had a slight impact on T-cell development in the thymus (Supplementary Fig. S15A and S15B). Specifically, CMTM6 deficiency slightly raised the proportion of $CD4^+CD8^-$ T cells, slightly decreased the proportion of $CD4^+CD8^+$ T cells, and increased the proportion of DN4 cells. Furthermore, freshly isolated thymic T cells from CMTM6-deficient mice also showed an increased pre-activated phenotype indicated by the expression of CD69 (Supplementary Fig. S15C). However, the development and preactivation phenotype of T cells in the spleen of CMTM6-deficient mice did not differ from WT mice (Supplementary Fig. S15D and S15E). Notably, $CD4^+$ T cells and $CD8^+$ T cells from the spleen of CMTM6-deficient mice were significantly higher in expression of CD44, CD69, IFNγ, and TNFα than T cells from WT mice after being isolated and stimulated with PMA and ionomycin for 24 hours, suggesting a higher activation state (Supplementary Fig. S16). These results suggest that CMTM6 has a potential regulatory effect on T-cell development and preactivation in the thymus but does not affect T-cell development and preactivation in the spleen. In addition, it suggests that CMTM6 may be associated with negative regulation of T-cell activation levels.

Considering the important role of NK cells in CMTM6-deficient tumors, we also tested whether NK-cell CMTM6 deficiency affects their development, preactivation, activation, and killing activity. CMTM6 deficiency did not affect the proportion of NK cells in the mouse spleen, but it did promote NK-cell development to $CD11b^+CD27^-$ cells (Supplementary Fig. S17A and S17B). CMTM6 deficiency also did not affect the preactivation phenotype of NK cells (Supplementary Fig. S17C). However, when activated by PMA and ionomycin or IL2, the activation markers of $CMTM6^{-/-}$ NK cells were not only not significantly upregulated, but some indicators, such as TNFα, were even significantly downregulated (Supplementary

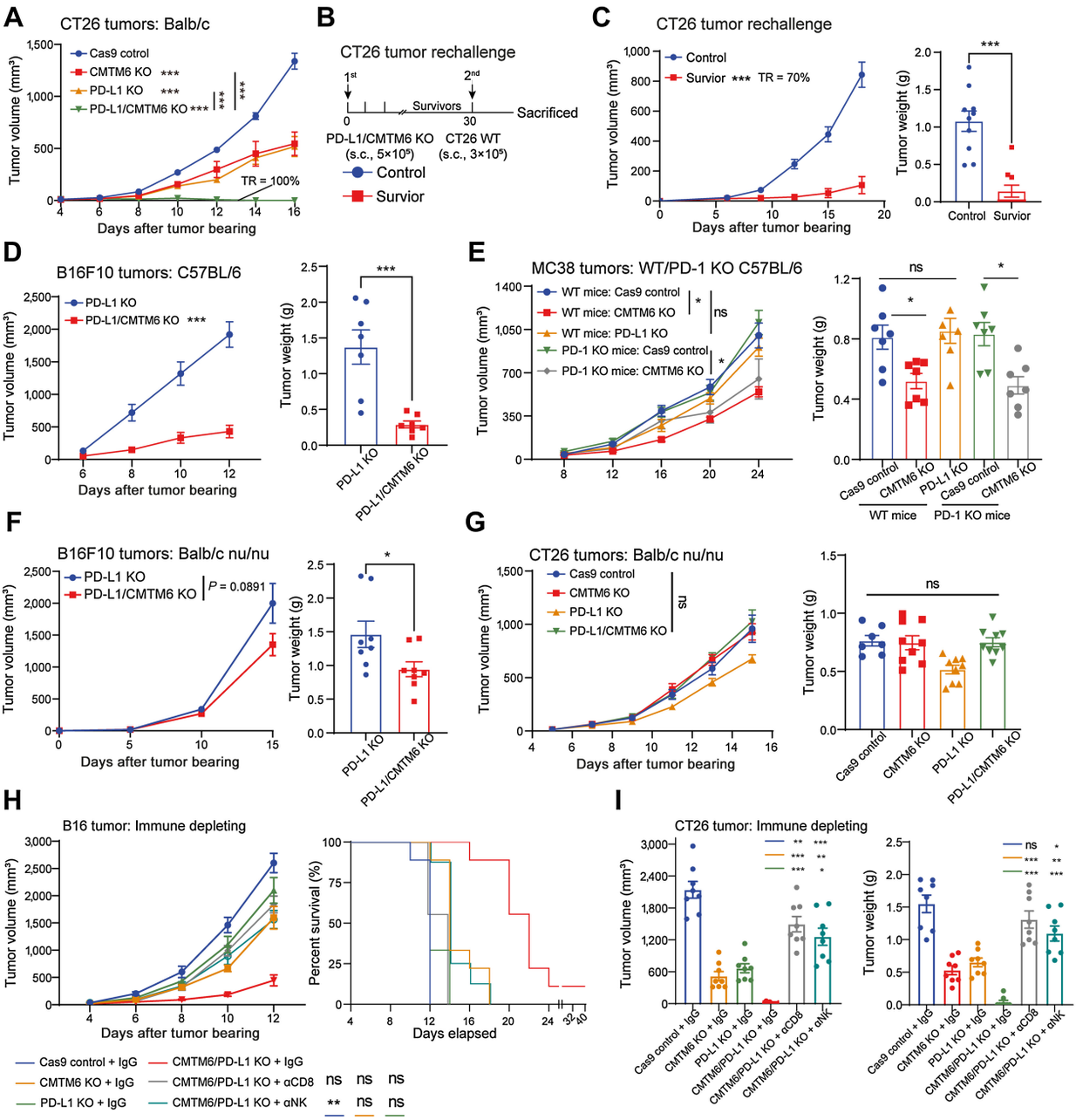

Figure 4.
CMTM6 could participate in tumor immunity independently of the PD-1/PD-L1 axis. **A,** Tumor growth kinetics of Cas9 control, CMTM6 KO, PD-L1 KO, and PD-L1/CMTM6 KO CT26 cells in Balb/c mice ($n = 10$). **B,** Schematic of the rechallenge schedules of mice with regressed tumors. **C,** Tumor volume and weight are shown ($n = 10$) for the CT26 rechallenge study. **D,** Tumor growth kinetics and weights of PD-L1 KO and PD-L1/CMTM6 KO B16F10 cells in C57BL/6 mice ($n = 7$). **E,** Tumor growth kinetics and weights of Cas9 control and PD-L1 KO MC38 cells in C57BL/6 mice or PD-1$^{-/-}$ mice ($n = 7$). **F,** Tumor growth kinetics and weights of PD-L1 KO and PD-L1/CMTM6 KO B16F10 cells in Balb/c nu/nu mice ($n = 8$). **G,** Tumor growth kinetics and weights of Cas9 control, CMTM6 KO, PD-L1 KO, and PD-L1/CMTM6 KO CT26 cells in Balb/c nu/nu mice ($n = 7$). **H,** C57BL/6 mice were dosed with immune cell depletion reagents and administered Cas9 control, CMTM6 KO, PD-L1 KO, or PD-L1/CMTM6 KO B16F10 tumors. Tumor volume and survival curves are shown ($n = 8$). **I,** Balb/c mice were dosed with immune cell depletion reagents and administered Cas9 control, CMTM6 KO, PD-L1 KO, or PD-L1/CMTM6 KO CT26 tumors. Tumor volume and weight are shown ($n = 8$). The data are presented as the mean ± SEM. *, $P < 0.05$; **, $P < 0.01$; ***, $P < 0.001$; ns not significant by an unpaired t test or one-way ANOVA followed by the Tukey multiple comparisons test.TR, tumor regression.

Fig. S17D and S17E). Furthermore, CMTM6 deficiency also did not increase NK-cell killing of YAC-1 cells and even showed a tendency to decrease killing activity in the 10:1 group (Supplementary Fig. S17F). Unlike T cells, these data suggest that CMTM6 may not be a negative regulator of NK activation.

The effect of host CMTM6 deficiency on tumor growth depends on CD8$^+$ T cells

To evaluate the effect of host CMTM6 deficiency on tumor development, we monitored the growth of B16F10 and MC38 tumors in CMTM6$^{-/-}$, CMTM6$^{-/+}$, and CMTM6$^{-/-}$ mice (**Fig. 6A**). The individual tumor growth kinetics and survival curves of B16F10 tumor-bearing mice showed that the higher the defective level of host CMTM6 the stronger the tumor growth inhibition. Similarly, MC38 tumor development was significantly constrained in both CMTM6$^{-/+}$ and CMTM6$^{-/-}$ mice compared with MC38 tumors in WT mice, with an IR of 27.5% and 54.7%, respectively (**Fig. 6B**).

To further investigate the effect of CMTM6 deficiency in host immune cells on their antitumor activity, we isolated splenocytes from CMTM6$^{+/+}$, CMTM6$^{-/+}$, and CMTM6$^{-/-}$ mice and transfused them back into MC38 tumors in NSG mice (**Fig. 6C**). The tumor growth curves showed that significant discrepancies in growth kinetics occurred between the three groups after transfusion. Splenocytes from CMTM6$^{-/-}$ mice inhibited MC38 tumors most effectively, suggesting that CMTM6 deficiency enhanced the antitumor activity of the immune system. Then, MC38 tumor-bearing CMTM6$^{-/-}$ mice were given immune cell-depleting antibodies to remove intratumoral CD4$^+$ T cells, CD8$^+$ T cells, or NK cells. The results showed that the intratumoral infiltration defect of CD8$^+$ T cells largely erased the tumor inhibitory effect in CMTM6-deficient mice (**Fig. 6D**). NK cells, although significantly affecting *in vivo* tumor suppression by tumor CMTM6 deficiency, played a minor role in host CMTM6 deficiency affecting tumor growth, which was also consistent with our analysis of the effect of CMTM6 on the activation and killing activity of NK cells. Furthermore, infusion of splenic T cells into MC38 tumors in C57BL/6 mice revealed that both CMTM6 partially and fully defective T cells significantly limited tumor growth (**Fig. 6E**).

The above results demonstrate that host CMTM6 affects tumor growth, especially in immune cells represented by CD8$^+$ T cells. Deficiency of CMTM6 can facilitate the antitumor activity of immune cells as the level of deficiency deepens.

T-cell CMTM6 expression is associated with exhaustion phenotypes

We speculated that CMTM6 was associated with tumor immunosuppression or exhaustion. By analyzing published pan-cancer tumor-infiltrating T-cell single-cell sequencing data (55), we found a propensity for CMTM6 expression in Tregs as well as in exhausted CD8$^+$ T cells (Tex; **Fig. 6F** and **G**). We did not observe PD-L1 upregulation in CD8$^+$ Tex, although we noticed a high expression of PD-L1 in Tregs (Supplementary Fig. S18). We then analyzed the CMTM6 expression profile of MC38 tumor-infiltrating WT T cells by flow cytometry. We found higher levels of CMTM6 expression in Tregs, CD25$^+$, PD-1$^+$, PD-L1$^+$, CTLA-4$^+$, and lymphocyte-activation gene 3 (LAG-3)$^+$ T cells (**Fig. 6H**). This coexpression with immunosuppressive molecules was more pronounced in CD4$^+$ T cells than in CD8$^+$ T cells. Further, we examined the proportion and function of immune cell subsets in MC38 tumors of CMTM6-deficient mice. The results showed significant downregulation of CD4$^+$ T cells and CD8$^+$ T cells expressing PD-1$^+$, PD-L1$^+$, CTLA-4$^+$, LAG-3$^+$, a decrease in Treg infiltration, an increase in CD8$^+$ T-cell infiltration and a significant increase in FasL$^+$, granzyme B$^+$, IFNγ^+ CD8$^+$ T cells in MC38 tumors from CMTM6-deficient mice compared with those from WT mice (**Fig. 6I**). These results suggest a link between CMTM6 and the exhaustion phenotype of tumor-infiltrating T cells, and that defects in CMTM6 in host immune cells can lessen immunosuppression and augment cytotoxic effects.

Host CMTM6 deficiency inhibits tumor growth in the absence of the PD-1/PD-L1 axis

In PD-L1$^{-/-}$ mice, we also aimed to investigate the biofunction of host CMTM6. We constructed CMTM6/PD-L1 double-knockout mice by breeding CMTM6 KO mice with PD-L1 KO mice (**Fig. 6J**). Compared with PD-L1 KO mice and CMTM6 KO mice, B16F10 tumors in CMTM6/PD-L1 KO mice grew more slowly and had a lower tumor weight with an IR of 70.8% compared with WT mouse tumors (**Fig. 6K**). Then we isolated splenocytes from WT, CMTM6 KO, PD-1 KO, and CMTM6/PD-L1 KO mice and transfused them back into MC38 tumors in NSG mice. The CMTM6/PD-L1 KO splenocyte transfusion inhibited tumor growth more significantly than the PD-L1 KO splenocyte transfusion, suggesting that CMTM6 ablation from host immune cells could mediate antitumor immunity independent of PD-L1 (**Fig. 6L**).

scAAV-mediated CMTM6 suppression is an effective tumor immunotherapy

In accordance with our finding that ablation of tumor or host CMTM6 could promote antitumor responses, we developed an scAAV9 encoding *Cmtm6* mRNA–targeting shRNA to mediate tumor gene therapy through CMTM6 suppression. The genomic patterns of the involved scAAVs are provided in Supplementary Fig. S19A. *In vitro*, the scAAV9-shCMTM6 effectively infected CT26 and B16F10 tumor cells and interfered with CMTM6 expression (Supplementary Fig. S19). *In vivo*, analysis of EGFP and CMTM6 expression within CT26 tumors 3 days after injection revealed that the scAAV9-shCMTM6 infected mainly tumor cells and only slightly infected immune cells (Supplementary Fig. S20).

CT26, B16F10, and Hepa1-6 tumor-bearing mice were administered with shNC scAAV9 and shCMTM6 scAAV9 on days 4, 6, and 8 (**Fig. 7A**). In terms of growth kinetics and tumor weight, shCMTM6 scAAV9 successfully halted tumor progression with IRs of 48.9%, 58.8%, and 50.6% against CT26, B16F10, and Hepa1-6 tumors, respectively (**Fig. 7B–D**). In addition, we generated an scAAV9 encoding both shCMTM6 and shPD-L1, and *in vivo* treatment experiments showed that shCMTM6&PD-L1 scAAV9 exerted superior antitumor efficacy over shCMTM6 scAAV9 and shPD-L1 scAAV9 with an IR of 76.4% (**Fig. 7E** and **F**). Immunophenotyping was performed to determine the proportion of immune cells in the tumor after scAAV9 treatment. The results showed that both shCMTM6 scAAV9 and shCMTM6&PD-L1 scAAV9 reduced PD-L1 levels in tumor cells and myeloid cells, decreased LAG-3, PD-1, PD-L1 expression in CD8$^+$ T cells, and promoted infiltrating CD8$^+$ T cells to express granzyme B, IFNγ, perforin, and TNFα (**Fig. 7G**). In addition, shCMTM6 and PD-L1 scAAV9 had a more significant effect on the TME.

scAAV-mediated CMTM6 suppression is effective in combination therapy

We next tried to combine shCMTM6 scAAV9 with the anti–PD-L1 atezolizumab, the TLR7 agonist imiquimod, the chemotherapeutic

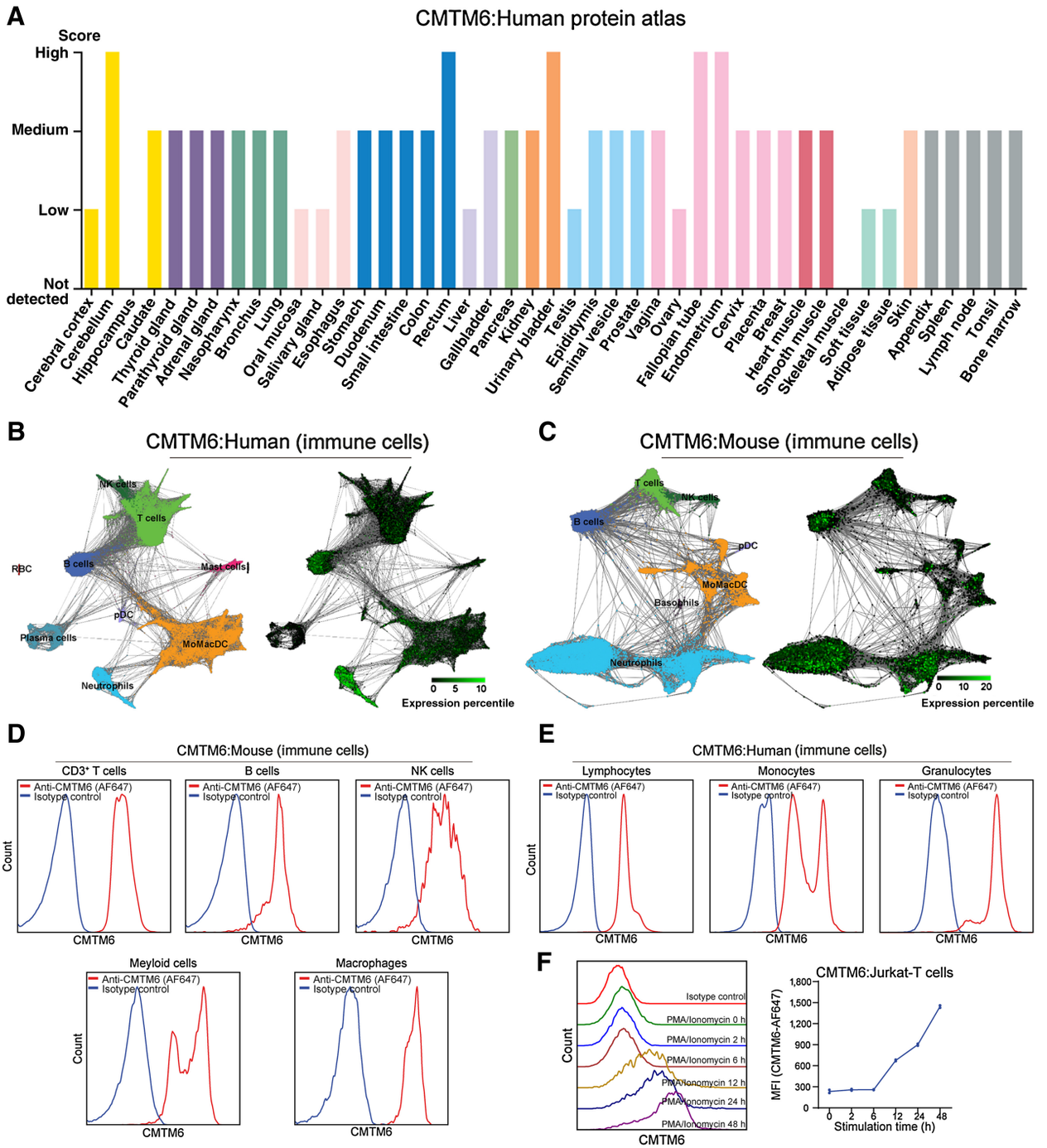

Figure 5.

T cell–intrinsic CMTM6 regulated PD-L1 expression. **A,** Data from the Human Protein Atlas Project were analyzed to determine the expression of human CMTM6 protein in tissues of the whole body. **B** and **C,** At the single-cell transcription level (GSE127465), the expression of murine (**B**) and human (**C**) CMTM6 in immune cells was analyzed. **D,** Histograms show CMTM6 expression in different mouse spleen immune cells measured by flow cytometry ($n = 3$). **E,** Histograms show CMTM6 expression in different human PBMC subsets by flow cytometry ($n = 3$). **F,** Histograms and line plot show CMTM6 expression in Jurkat cells stimulated with PMA and ionomycin for different times measured by flow cytometry ($n = 3$). (*Continued on the following page.*)

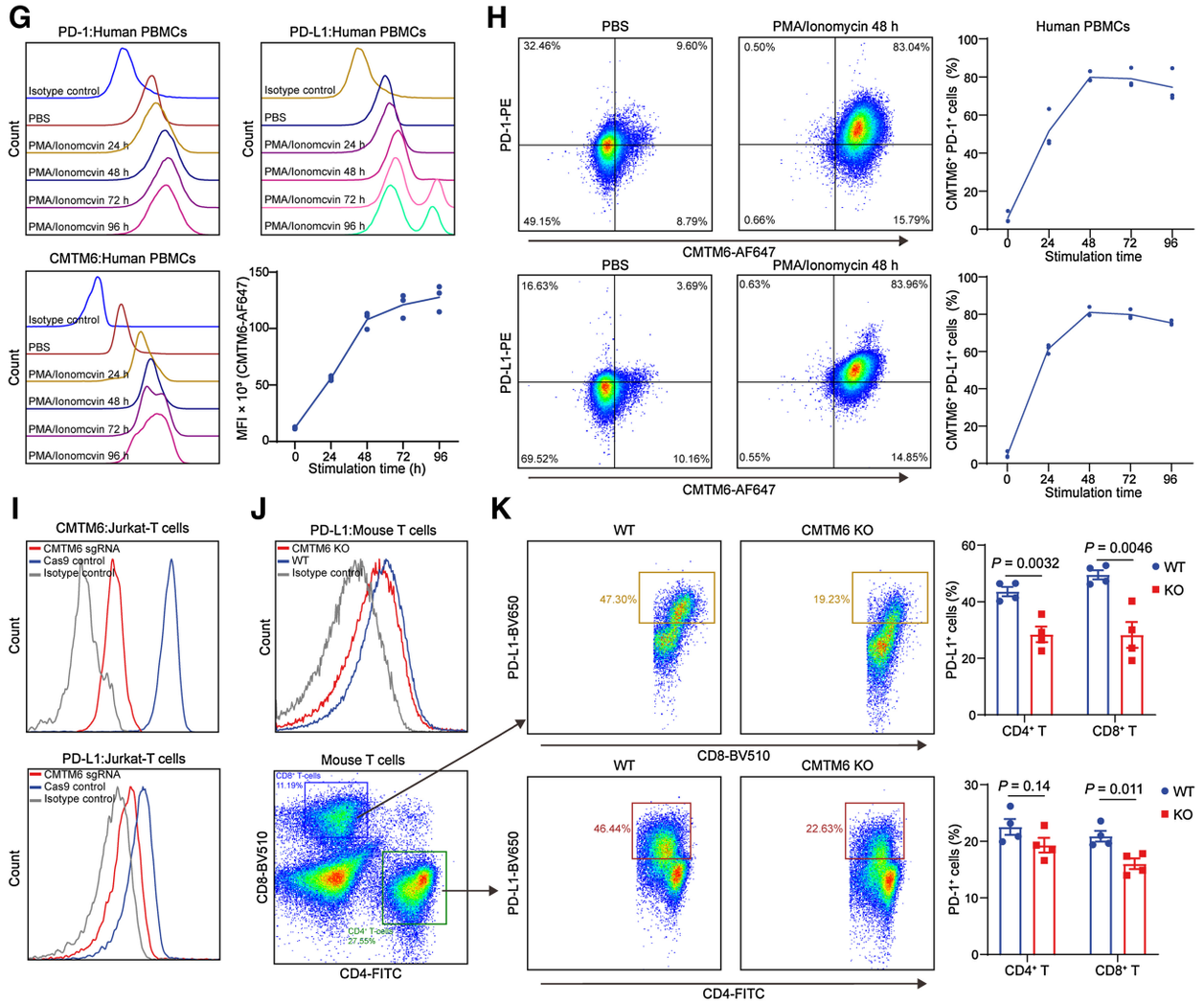

Figure 5.

(*Continued.*) **G,** Histograms and line plot show CMTM6, PD-1, and PD-L1 expression in human PBMCs stimulated with PMA and ionomycin for different times measured by flow cytometry ($n = 3$). **H,** Density plots and line plots show coexpression of CMTM6/PD-1 and CMTM6/PD-L1 in human PBMCs stimulated with PMA and ionomycin for different times measured by flow cytometry ($n = 3$). **I,** Top, identification of CMTM6 knockout Jurkat cells. Bottom, difference in PD-L1 expression between Cas9 control and CMTM6 KO Jurkat cells stimulated by PMA and ionomycin. **J,** The histogram shows the difference in PD-L1 expression between WT and CMTM6 KO murine $CD3^+$ T cells stimulated by PMA and ionomycin. **K,** Density plots and scatter plots show the difference in PD-L1 and PD-1 expression between WT and CMTM6 KO murine $CD4^+$ T cells and $CD8^+$ T cells stimulated by PMA and ionomycin ($n = 4$). The data are presented as the mean ± SEM and analyzed by two-way ANOVA followed by the Tukey multiple comparisons test.

drug doxorubicin, the antidiabetic drug metformin, and the antilipemic drug fluvastatin to further explore the value of shCMTM6 scAAV9 application (**Fig. 7H**). These combination strategies represent the combination of immune-checkpoint inhibitors, immune agonists, chemotherapeutic agents, and metabolic modulating agents, respectively. In the CT26 tumor model, we found that all selected combinations achieved significantly better antitumor activity than single agents. Although none showed synergistic efficacy, the combinations did exert potent tumor-suppressive effects, particularly shCMTM6 scAAV9 in combination with doxorubicin and shCMTM6 in combination with fluvastatin with IRs of 83.1% and 63.3%, respectively. We also tested shCMTM6 scAAV9 in combination with low doses of the chemotherapeutic agents doxorubicin or cisplatin, and the effect of the combination remained impressive, although still not synergistic (Supplementary Fig. S21). The enhanced efficacy achieved by these classic combination strategies also hints at cross-talk between tumor CMTM6 inhibition and biological processes such as lipid metabolism and gene synthesis. The failure of shCMTM6 scAAV9 in combination with atezolizumab to demonstrate CMTM6/PD-L1 knockout-like efficacy may be due to the limited gene knockdown efficiency of shRNA-AAV. The above results demonstrate that the shCMTM6 scAAV9 we developed can effectively mediate tumor immunotherapy and be applied in combination. CMTM6 is a novel tumor immunotherapy target with great clinical application potential.

Discussion

After studying the role of CMTM6 in regulating tumor development and immunity in this work, we developed an AAV-mediated CMTM6-targeting gene therapy, confirming the potential of this previously unexplored target. Other gene therapy approaches could also be wielded to target CMTM6, such as oncolytic viruses and siRNA-loaded liposomes. In addition to gene therapy, classic antibodies and small molecules are also expected to be screened for interfering with CMTM6 function. Because CMTM6 is a four-transmembrane protein and its extracellular segment is predicted

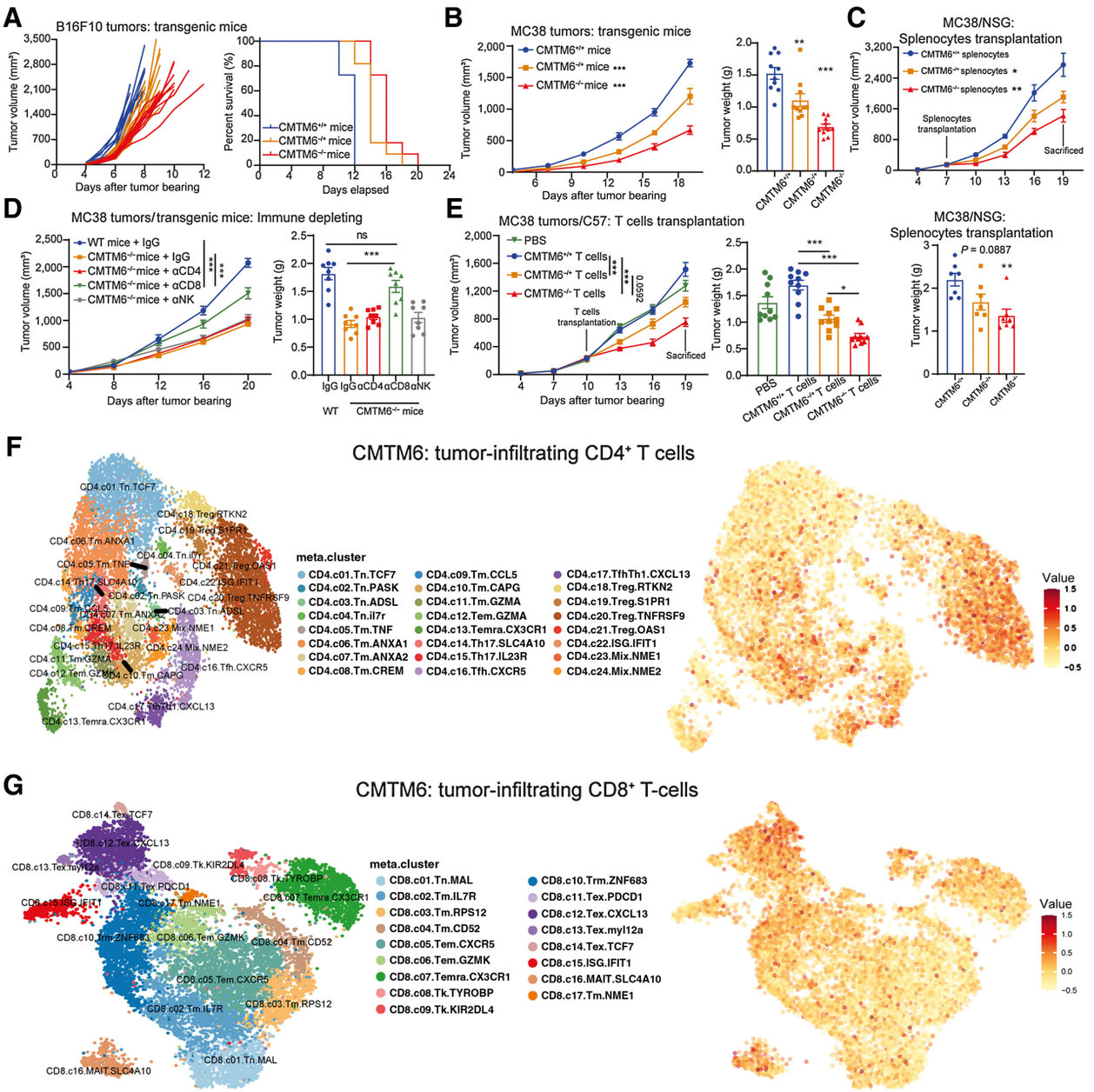

Figure 6.

Host CMTM6 was associated with T-cell exhaustion and host CMTM6 knockout could enhance antitumor immunity independently of PD-L1. **A,** Individual growth curves are shown for B16F10 tumors in CMTM6$^{+/+}$, CMTM6$^{-/+}$, and CMTM6$^{-/-}$ mice (left; $n = 8$). Right, Kaplan–Meier plot of survival. **B,** Tumor growth kinetics and weights of MC38 cells in CMTM6$^{+/+}$, CMTM6$^{-/+}$, and CMTM6$^{-/-}$ mice ($n = 10$). **C,** Tumor growth kinetics and weights of MC38 cells in NSG mice injected with CMTM6$^{+/+}$, CMTM6$^{-/+}$, and CMTM6$^{-/-}$ splenocytes ($n = 7$). **D,** WT and CMTM6$^{-/-}$ mice were dosed with immune cell depletion reagents and administered MC38 tumors. Tumor volume and weight are shown ($n = 8$). **E,** Tumor growth kinetics and weights of MC38 cells in C57BL/6 mice injected with CMTM6$^{+/+}$, CMTM6$^{-/+}$, and CMTM6$^{-/-}$ T cells ($n = 10$). **F** and **G,** Single-cell RNA-seq data for CMTM6 expression in tumor-infiltrating CD4^{+} (**F**) and CD8^{+} (**G**) T cells. (*Continued on the following page.*)

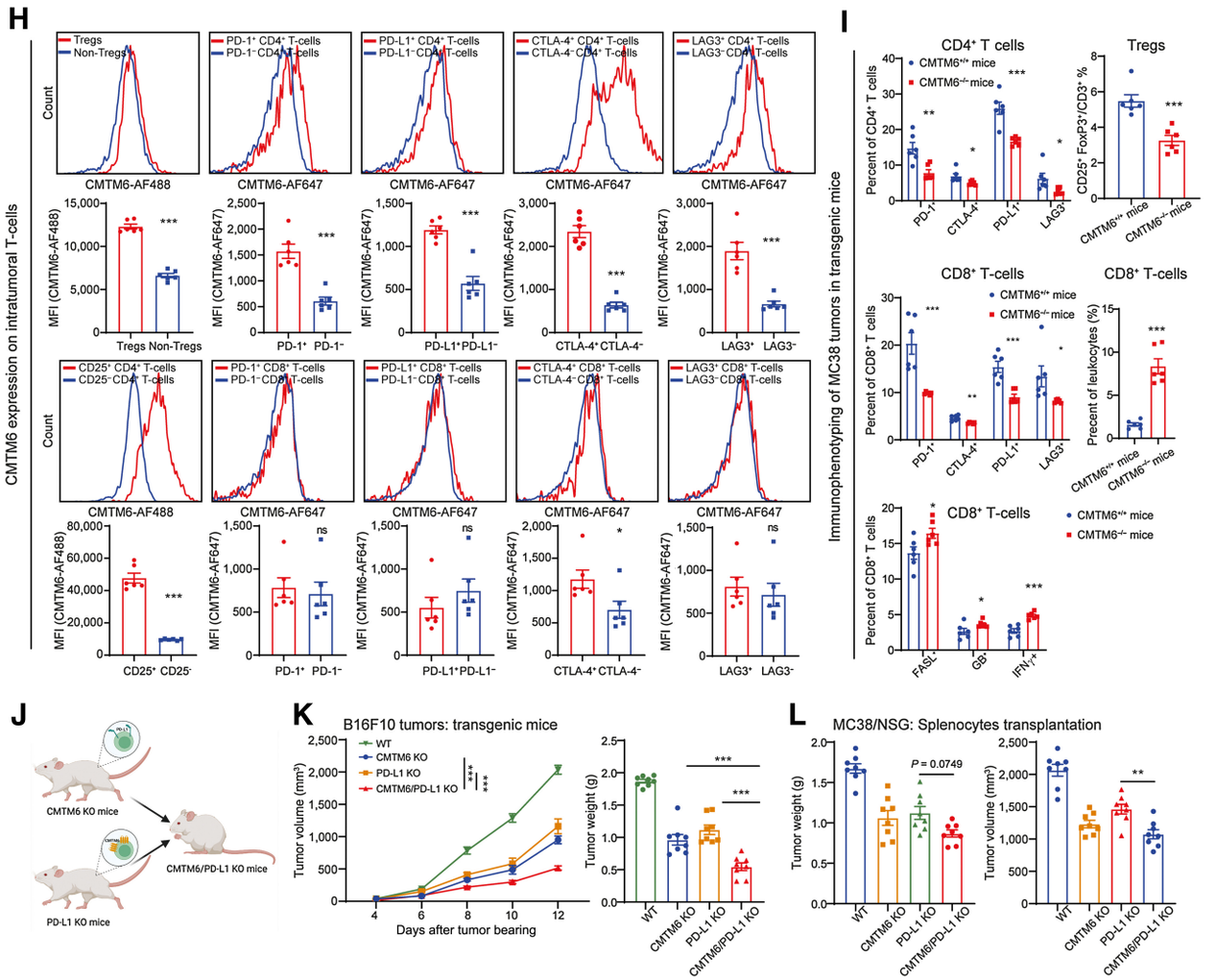

Figure 6.

(*Continued.*) **H,** Differences in CMTM6 expression in immune cells isolated from MC38 tumors in WT and CMTM6$^{-/-}$ mice (n = 6). **I,** At 19 days after tumor administration, immune effector cells from MC38 tumors in WT and CMTM6$^{-/-}$ mice were quantified by flow cytometry (n = 6). The percentages of specific CD4$^+$ and CD8$^+$ T cells are shown based on their respective markers. **J,** The schematic diagram shows the breeding of CMTM6/PD-L1 KO mice. **K,** Tumor growth kinetics and weights of B16F10 cells in WT, CMTM6 KO, PD-L1 KO, and CMTM6/PD-L1 KO mice (n = 8). **L,** Tumor weight and volume of MC38 tumors in NSG mice injected with WT, CMTM6 KO, PD-L1 KO, and CMTM6/PD-L1 KO splenocytes (n = 8) are shown. Data, mean ± SEM. *, $P < 0.05$; **, $P < 0.01$; *** $P < 0.001$; ns, not significant by an unpaired t test or one-way/two-way ANOVA followed by the Tukey multiple comparisons test.

to be two little loops comprising only seven amino acids each, generating CMTM6-specific antibodies will likely be development challenges. In addition, whether and how antibodies directly bound to CMTM6 can function still needs to be systematically evaluated. We postulate that affecting the CMTM6/PD-L1 interaction is one of the possible mechanisms by which anti-CMTM6 might function. Tailoring antibodies to link lysosomal-targeting peptides or ligands of cell-surface lysosomal-targeting receptors is a promising direction to achieve direct degradation of CMTM6, which is consistent with the strategy of gene therapy. In addition, considering that the shCMTM6-scAAV9 we developed mainly infects tumor cells *in vivo*, modification of the AAV capsid with targeted peptides or antibodies (56) against T cells and other immune cells is a potential way to broaden application and improve efficacy.

Considering the efficacy of CMTM6 knockout and shCMTM6 scAAV in pan-tumors, the CMTM6-targeted therapies discussed above have broad clinical potential. Moreover, we also observed that CMTM6 knockout reversed ICB treatment resistance in two murine tumor models. Although knockout of tumor CMTM6 can lead to decreased tumor PD-L1 expression, there are still various cells with high PD-L1 expression in the TME that can be targeted by anti–PD-L1, such as myeloid cells and T cells. In recent years, several studies have also reported that PD-L1$^+$ myeloid cells or T cells contribute to anti–PD-L1 efficacy in some tumors (54, 57, 58). In addition, tumor CMTM6 deficiency promotes intratumoral immune cell infiltration and function, allowing the tumor to shift from "cold" to "hot," which also contributes to the efficacy of ICB therapy.

We found that the suppression of host/tumor CMTM6 contained tumor development incompletely dependent on PD-L1. In the

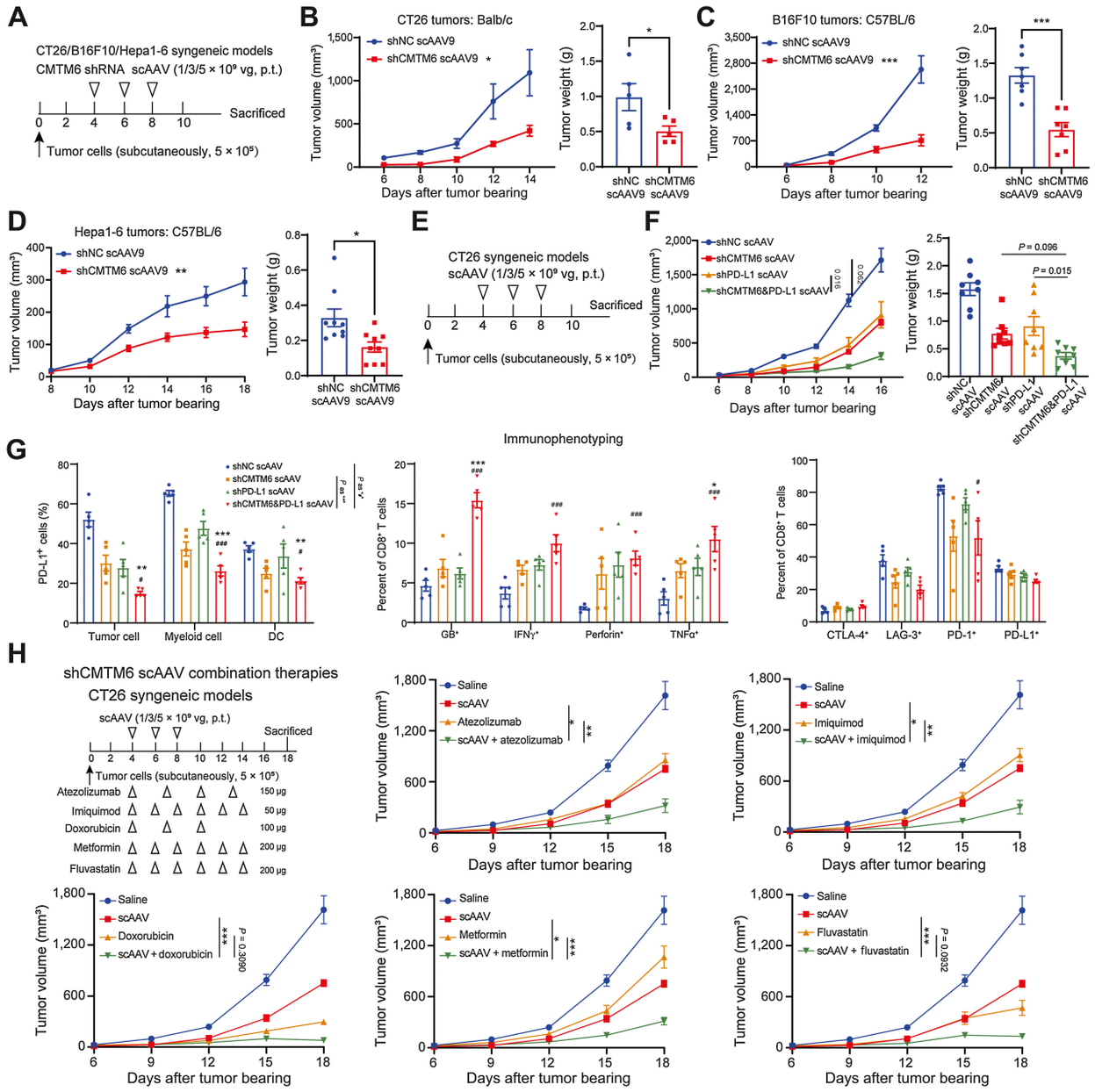

Figure 7.

scAAV-mediated CMTM6 suppression was effective in tumor immunotherapy and combination therapy. **A,** Schematic of treatment schedules and dosing of shNC and shCMTM6 scAAV9 in mice bearing CT26, B16F10, or Hepa1-6 tumors. **B–D,** Tumor growth kinetics and weights of CT26 (**B**), B16F10 (**C**), and Hepa1-6 cells (**D**) in mice treated with shNC or shCMTM6 scAAV9. **E,** Schematic of treatment schedules and dosing of shNC, shCMTM6, shPD-L1, and shCMTM6&PD-L1 scAAV9 in mice bearing CT26 tumors. **F,** Tumor growth kinetics and weights of CT26 cells in mice treated with shNC, shCMTM6, shPD-L1, or shCMTM6&PD-L1 scAAV9 ($n = 8$). **G,** At 16 days after tumor administration, immune effector cells from CT26 tumors in mice treated with shNC, shCMTM6, shPD-L1, or shCMTM6&PD-L1 scAAV9 were quantified by flow cytometry ($n = 5$). The percentages of specific $CD8^+$ T cells are shown based on their respective markers. **H,** Schematic of combination treatment schedules in mice bearing CT26 tumors are shown. Tumor growth kinetics of CT26 cells in mice treated with different combination strategies are shown ($n = 8$). Data, mean ± SEM. *, $P < 0.05$; **, $P < 0.01$; ***, $P < 0.001$; ns, not significant by an unpaired *t* test or one-way/two-way ANOVA followed by the Tukey multiple comparisons test.

MC38 tumor model, PD-L1 knockout did not affect tumor growth *in vivo* at all, whereas CMTM6 knockout could significantly repress tumors, which suggests that CMTM6 inhibition can exert tumor modulation completely independent of PD-L1. Thus, CMTM6 can function independently of PD-L1 as a tumor growth and immune-regulating molecule. We also found that CMTM6 affected Akt/GSK3β/β-catenin signaling independently of PD-L1, which was consistent with a previous report (34). Tumor CMTM6 may be

involved in antitumor immunity by regulating CCL4 expression through modulation of β-catenin signaling to influence intratumoral $CD8^+$ T-cell infiltration. Of course, how CMTM6 regulates Akt/GSK3β/β-catenin signaling is not clear, and the mechanism by which CMTM6 regulates antitumor immunity independent of PD-L1 still needs to be further explored. We also hypothesized that CMTM6 might affect the stability of other immune-related membrane proteins. And as a MARVEL domain-containing membrane protein, CMTM6 may also be involved in regulating processes such as vesicle transport and tight junctions (11). In addition, some recently discovered potential interaction molecules and functions of CMTM6 (35–39) are also potential explanations. These findings warrant further investigation to ascertain the circumstances under which CMTM6 functions independently of PD-L1.

Considering that T cells play a major antitumor role in CMTM6-deficient mice, we focused on the function of T cell–intrinsic CMTM6. However, single-cell sequencing results showed that CMTM6 was widely expressed in other immune cells, and it was in fact predominated in granulocytes and macrophages. For example, Markus Zeisbrich and colleagues found that CMTM6 in monocytes can affect the expression of membrane PD-L1 (13). Therefore, on other immune cells, whether CMTM6 regulates PD-L1 stability and whether it depends on PD-L1 for its functions needs to be systematically investigated.

Our present study has some limitations, and we plan to address those issues in further research. First, because the *in vivo* experiments all used subcutaneous tumor models, and as *in situ* tumors can more realistically reflect the biofunctions, we plan to construct CMTM6-deficient *in situ* tumor models for further studies. Second, the evaluation of shCMTM6-scAAV9 is not yet complete. The efficacy needs to be evaluated in more tumor models and *in situ* tumor models, and the long-term efficacy and safety of this therapy need to be paid attention to. Third, we plan to further explore the molecules regulated by CMTM6 besides PD-L1, as well as the functions of CMTM6 on other immune cells to further substantiate the conclusions of this paper mechanistically.

In summary, based on the clinical relevance of CMTM6, this work analyzed and characterized CMTM6 expression profiles and the association between immune exhaustion phenotypes, and systematically investigated tumor/host CMTM6 in the regulation of tumor progression and tumor immunity in pan-cancer. Both host and tumor CMTM6 deficiency can reshape the antitumor immune microenvironment, which is mainly dependent on cytotoxic cells, in a PD-L1 nondependent manner. In addition, in this study, we developed CMTM6-targeted gene therapy and demonstrated its potent pan-cancer efficacy for immunotherapy and manifold combinations. CMTM6 is a novel target with great potential for antitumor immunotherapy.

Authors' Disclosures

Y. Long, R. Chen, X. Yu, X. Peng, F. Li, C. Hu, J. Sun, and L. Gong report grants from the Foundation of Shanghai Science and Technology Committee, the Zhongshan Municipal Bureau of Science and Technology, the Department of Science and Technology of Guangdong Province, and the Strategic Priority Research Program of the Chinese Academy of Sciences during the conduct of the study. No disclosures were reported by the other authors.

Authors' Contributions

Y. Long: Conceptualization, resources, data curation, software, formal analysis, investigation, visualization, methodology, writing–original draft, project administration, writing–review and editing. **R. Chen:** Resources, validation, investigation, writing–review and editing. **X. Yu:** Supervision, validation, investigation. **Y. Tong:** Software, investigation. **X. Peng:** Investigation. **F. Li:** Investigation. **C. Hu:** Investigation. **J. Sun:** Conceptualization, resources, supervision, investigation, writing–review and editing. **L. Gong:** Conceptualization, resources, data curation, formal analysis, supervision, funding acquisition, validation, writing–original draft, project administration, writing–review and editing.

Acknowledgments

We thank Professor Y. Geng for scientific discussions. All the figures were created with BioRender.com. This work was supported by the Foundation of Shanghai Science and Technology Committee (No. 22S11902100), the Zhongshan Municipal Bureau of Science and Technology (No. 2020SYF08), the Department of Science and Technology of Guangdong Province (No. 2019B090904008 and No. 2021B0909050003), and the Strategic Priority Research Program of the Chinese Academy of Sciences (No. XDA 12050305).

The publication costs of this article were defrayed in part by the payment of publication fees. Therefore, and solely to indicate this fact, this article is hereby marked "advertisement" in accordance with 18 USC section 1734.

Note

Supplementary data for this article are available at Cancer Immunology Research Online (http://cancerimmunolres.aacrjournals.org/).

Received May 30, 2022; revised September 3, 2022; accepted December 2, 2022; published first December 8, 2022.

References

1. Brahmer JR, Tykodi SS, Chow LQM, Hwu W-J, Topalian SL, Hwu P, et al. Safety and activity of anti–PD-L1 antibody in patients with advanced cancer. 2012;366:2455–65.
2. Powles T, Eder JP, Fine GD, Braiteh FS, Loriot Y, Cruz C, et al. MPDL3280A (anti-PD-L1) treatment leads to clinical activity in metastatic bladder cancer. Nature 2014;515:558–62.
3. Rosenberg JE, Hoffman-Censits J, Powles T, van der Heijden MS, Balar AV, Necchi A, et al. Atezolizumab in patients with locally advanced and metastatic urothelial carcinoma who have progressed following treatment with platinum-based chemotherapy: a single-arm, multicentre, phase 2 trial. Lancet North Am Ed 2016;387:1909–20.
4. Schmid P, Adams S, Rugo HS, Schneeweiss A, Barrios CH, Iwata H, et al. Atezolizumab and nab-paclitaxel in advanced triple-negative breast cancer. N Engl J Med 2018;379:2108–21.
5. Socinski MA, Jotte RM, Cappuzzo F, Orlandi F, Stroyakovskiy D, Nogami N, et al. Atezolizumab for first-line treatment of metastatic nonsquamous NSCLC. N Engl J Med 2018;378:2288–301.
6. Kornepati AVR, Vadlamudi RK, Curiel TJ. Programmed death ligand 1 signals in cancer cells. Nat Rev Cancer 2022;22:174–89.
7. Gou Q, Dong C, Xu H, Khan B, Jin J, Liu Q, et al. PD-L1 degradation pathway and immunotherapy for cancer. Cell Death Dis 2020;11:955.
8. Burr ML, Sparbier CE, Chan YC, Williamson JC, Woods K, Beavis PA, et al. CMTM6 maintains the expression of PD-L1 and regulates anti-tumour immunity. Nature 2017;549:101–5.
9. Mezzadra R, Sun C, Jae LT, Gomez-Eerland R, de Vries E, Wu W, et al. Identification of CMTM6 and CMTM4 as PD-L1 protein regulators. Nature 2017;549:106–10.
10. Han W, Ding P, Xu M, Wang L, Rui M, Shi S, et al. Identification of eight genes encoding chemokine-like factor superfamily members 1–8 (CKLFSF1–8) by in silico cloning and experimental validation. Genomics 2003;81:609–17.
11. Sánchez-Pulido L, Martín-Belmonte F, Valencia A, Alonso MA. MARVEL: a conserved domain involved in membrane apposition events. Trends Biochem Sci 2002;27:599–601.

12. Jin C, Ding P, Wang Y, Ma D. Regulation of EGF receptor signaling by the MARVEL domain-containing protein CKLFSF8. FEBS Lett 2005;579: 6375–82.
13. Zeisbrich M, Chevalier N, Sehnert B, Rizzi M, Venhoff N, Thiel J, et al. CMTM6-deficient monocytes in ANCA-associated vasculitis fail to present the immune checkpoint PD-L1. Front Immunol 2021;12:673912.
14. Takeuchi H, Konnai S, Maekawa N, Minato E, Ichikawa Y, Kobayashi A, et al. Expression analysis of canine CMTM6 and CMTM4 as potential regulators of the PD-L1 protein in canine cancers. Front Vet Sci 2020;7:330.
15. Shang X, Li J, Wang H, Li Z, Lin J, Chen D, et al. CMTM6 is positively correlated with PD-L1 expression and immune cells infiltration in lung squamous carcinoma. Int Immunopharmacol 2020;88:106864.
16. Zhao Y, Zhang M, Pu H, Guo S, Zhang S, Wang Y. Prognostic implications of pan-cancer CMTM6 expression and its relationship with the immune microenvironment. Front Oncol 2020;10:585961.
17. Ishihara S, Iwasaki T, Kohashi K, Yamada Y, Toda Y, Ito Y, et al. The association between the expression of PD-L1 and CMTM6 in undifferentiated pleomorphic sarcoma. J Cancer Res Clin Oncol 2021;147:2003–11.
18. Muranushi R, Araki K, Yokobori T, Chingunjav B, Hoshino K, Dolgormaa G, et al. High membrane expression of CMTM6 in hepatocellular carcinoma is associated with tumor recurrence. Cancer Sci 2021;112:3314–23.
19. Tian Y, Sun X, Cheng G, Ji E, Yang S, Feng J, et al. The association of CMTM6 expression with prognosis and PD-L1 expression in triple-negative breast cancer. Ann Transl Med 2021;9:131.
20. Yugawa K, Itoh S, Yoshizumi T, Iseda N, Tomiyama T, Morinaga A, et al. CMTM6 stabilizes PD-L1 expression and is a new prognostic impact factor in hepatocellular carcinoma. Hepatol Commun 2021;5:334–48.
21. Guan X, Zhang C, Zhao J, Sun G, Song Q, Jia W. CMTM6 overexpression is associated with molecular and clinical characteristics of malignancy and predicts poor prognosis in gliomas. EBioMedicine 2018;35:233–43.
22. Chen L, Yang QC, Li YC, Yang LL, Liu JF, Li H, et al. Targeting CMTM6 suppresses stem cell-like properties and enhances antitumor immunity in head and neck squamous cell carcinoma. Cancer Immunol Res 2020;8:179–91.
23. Li X, Chen L, Gu C, Sun Q, Li J. CMTM6 significantly relates to PD-L1 and predicts the prognosis of gastric cancer patients. PeerJ 2020;8:e9536.
24. Martinez-Morilla S, Zugazagoitia J, Wong PF, Kluger HM, Rimm DL. Quantitative analysis of CMTM6 expression in tumor microenvironment in metastatic melanoma and association with outcome on immunotherapy. Oncoimmunology 2020;10:1864909.
25. Liu LL, Zhang SW, Chao X, Wang CH, Yang X, Zhang XK, et al. Coexpression of CMTM6 and PD-L1 as a predictor of poor prognosis in macrotrabecular-massive hepatocellular carcinoma. Cancer Immunol Immunother 2021;70: 417–29.
26. Wang Z, Peng Z, Liu Q, Guo Z, Menatola M, Su J, et al. Co-expression with membrane CMTM6/4 on tumor epithelium enhances the prediction value of PD-L1 on anti-PD-1/L1 therapeutic efficacy in gastric adenocarcinoma. Cancers 2021;13:5175.
27. Zhang C, Zhao S, Wang X. Co-expression of CMTM6 and PD-L1: a novel prognostic indicator of gastric cancer. Cancer Cell Int 2021;21:78.
28. Koh YW, Han JH, Haam S, Jung J, Lee HW. Increased CMTM6 can predict the clinical response to PD-1 inhibitors in non-small cell lung cancer patients. Oncoimmunology 2019;8:e1629261.
29. Zugazagoitia J, Liu Y, Toki M, McGuire J, Ahmed FS, Henick BS, et al. Quantitative assessment of CMTM6 in the tumor microenvironment and association with response to PD-1 pathway blockade in advanced-stage non-small cell lung cancer. J Thorac Oncol 2019;14:2084–96.
30. Wu X, Lan X, Hu W, Zhang W, Lai X, Xu S, et al. CMTM6 expression in M2 macrophages is a potential predictor of PD-1/PD-L1 inhibitor response in colorectal cancer. Cancer Immunol Immunother 2021;70:3235–48.
31. Zhu X, Qi G, Li C, Bei C, Tan C, Zhang Y, et al. Expression and clinical significance of CMTM6 in hepatocellular carcinoma. DNA Cell Biol 2019;38: 193–7.
32. Peng QH, Wang CH, Chen HM, Zhang RX, Pan ZZ, Lu ZH, et al. CMTM6 and PD-L1 coexpression is associated with an active immune microenvironment and a favorable prognosis in colorectal cancer. J Immunother Cancer 2021;9: e001638.
33. Yin B, Ding J, Hu H, Yang M, Huang B, Dong W, et al. Overexpressed CMTM6 improves prognosis and associated with immune infiltrates of ovarian cancer. Front Mol Biosci 2022;9:769032.
34. Mohapatra P, Shriwas O, Mohanty S, Ghosh A, Smita S, Kaushik SR, et al. CMTM6 drives cisplatin resistance by regulating Wnt signaling through the ENO-1/AKT/GSK3beta axis. JCI Insight 2021;6:e143643.
35. Pang X, Wang SS, Zhang M, Jiang J, Fan HY, Wu JS, et al. OSCC cell-secreted exosomal CMTM6 induced M2-like macrophages polarization via ERK1/2 signaling pathway. Cancer Immunol Immunother 2021;70:1015–29.
36. Huang Y, Zhu Y, Yang J, Pan Q, Zhao J, Song M, et al. CMTM6 inhibits tumor growth and reverses chemoresistance by preventing ubiquitination of p21 in hepatocellular carcinoma. Cell Death Dis 2022;13:251.
37. Wang H, Fan Y, Chen W, Lv Z, Wu S, Xuan Y, et al. Loss of CMTM6 promotes DNA damage-induced cellular senescence and antitumor immunity. Oncoimmunology 2022;11:2011673.
38. Wei L, Wei Q, Yang X, Zhou P. CMTM6 knockdown prevents glioma progression by inactivating the mTOR pathway. Ann Transl Med 2022;10:181.
39. Huang X, Xiang L, Wang B, Hu J, Liu C, Ren A, et al. CMTM6 promotes migration, invasion, and EMT by interacting with and stabilizing vimentin in hepatocellular carcinoma cells. J Transl Med 2021;19:120.
40. Liu Y, Li X, Zhang H, Zhang M, Wei Y. HuR up-regulates cell surface PD-L1 via stabilizing CMTM6 transcript in cancer. Oncogene 2021;40:2230–42.
41. Zheng Y, Wang C, Song A, Jiang F, Zhou J, Li G, et al. CMTM6 promotes cell proliferation and invasion in oral squamous cell carcinoma by interacting with NRP1. Am J Cancer Res 2020;10:1691–709.
42. Eichel MA, Gargareta V-I, D'Este E, Fledrich R, Kungl T, Buscham TJ, et al. CMTM6 expressed on the adaxonal Schwann cell surface restricts axonal diameters in peripheral nerves. Nat Commun 2020;11:4514.
43. Tang Z, Li C, Kang B, Gao G, Li C, Zhang Z. GEPIA: a web server for cancer and normal gene expression profiling and interactive analyses. Nucleic Acids Res 2017;45:W98–w102.
44. Li T, Fu J, Zeng Z, Cohen D, Li J, Chen Q, et al. TIMER2.0 for analysis of tumor-infiltrating immune cells. Nucleic Acids Res 2020;48:W509–W14.
45. Young TM, Reyes C, Pasnikowski E, Castanaro C, Wong C, Decker CE, et al. Autophagy protects tumors from T cell-mediated cytotoxicity via inhibition of TNFα-induced apoptosis. Sci Immunol 2020;5:eabb9561.
46. Kearney CJ, Vervoort SJ, Hogg SJ, Ramsbottom KM, Freeman AJ, Lalaoui N, et al. Tumor immune evasion arises through loss of TNF sensitivity. Sci Immunol 2018;3:eaar3451.
47. Lawson KA, Sousa CM, Zhang X, Kim E, Akthar R, Caumanns JJ, et al. Functional genomic landscape of cancer-intrinsic evasion of killing by T cells. Nature 2020;586:120–6.
48. Spranger S, Bao R, Gajewski TF. Melanoma-intrinsic β-catenin signalling prevents anti-tumour immunity. Nature 2015;523:231–5.
49. Casey SC, Tong L, Li Y, Do R, Walz S, Fitzgerald KN, et al. MYC regulates the antitumor immune response through CD47 and PD-L1. 2016;352:227–31.
50. Wong C, Chen C, Wu Q, Liu Y, Zheng P. A critical role for the regulated wnt-myc pathway in naive T cell survival. J Immunol 2015;194:158–67.
51. Uhlén M, Fagerberg L, Hallström BM, Lindskog C, Oksvold P, Mardinoglu A, et al. Proteomics: tissue-based map of the human proteome. Science 2015;347: 1260419.
52. Karlsson M, Zhang C, Méar L, Zhong W, Digre A, Katona B, et al. A single-cell type transcriptomics map of human tissues. Sci Adv 2021;7:eabh2169.
53. Zilionis R, Engblom C, Pfirschke C, Savova V, Zemmour D, Saatcioglu HD, et al. Single-cell transcriptomics of human and mouse lung cancers reveals conserved myeloid populations across individuals and species. Immunity 2019;50:1317–34.
54. Diskin B, Adam S, Cassini MF, Sanchez G, Liria M, Aykut B, et al. PD-L1 engagement on T cells promotes self-tolerance and suppression of neighboring macrophages and effector T cells in cancer. Nat Immunol 2020;21: 442–54.
55. Zheng L, Qin S, Si W, Wang A, Xing B, Gao R, et al. Pan-cancer single-cell landscape of tumor-infiltrating T cells. Science 2021;374:abe6474.
56. Li C, Samulski RJ. Engineering adeno-associated virus vectors for gene therapy. Nat Rev Genet 2020;21:255–72.
57. Lin H, Wei S, Hurt EM, Green MD, Zhao L, Vatan L, et al. Host expression of PD-L1 determines efficacy of PD-L1 pathway blockade-mediated tumor regression. J Clin Invest 2018;128:805–15.
58. Tang H, Liang Y, Anders RA, Taube JM, Qiu X, Mulgaonkar A, et al. PD-L1 on host cells is essential for PD-L1 blockade–mediated tumor regression. J Clin Invest 2018;128:580–8.